Monthly Notices
of the
ROYAL ASTRONOMICAL SOCIETY

MNRAS **456,** 1459–1483 (2016) doi:10.1093/mnras/stv2741

The evolution of the stellar mass versus halo mass relationship

Peter D. Mitchell,* Cedric G. Lacey, Carlton M. Baugh and Shaun Cole

Department of Physics, Institute for Computational Cosmology, University of Durham, South Road, Durham DH1 3LE, UK

Accepted 2015 November 19. Received 2015 October 27; in original form 2015 July 30

ABSTRACT

We present an analysis of the predictions made by the GALFORM semi-analytic galaxy formation model for the evolution of the relationship between stellar mass and halo mass. We show that for the standard implementations of supernova feedback and gas reincorporation used in semi-analytic models, this relationship is predicted to evolve weakly over the redshift range $0 < z < 4$. Modest evolution in the median stellar mass versus halo mass (SHM) relationship implicitly requires that, at fixed halo mass, the efficiency of stellar mass assembly must be almost constant with cosmic time. We show that in our model, this behaviour can be understood in simple terms as a result of a constant efficiency of gas reincorporation, and an efficiency of SNe feedback that is, on average, constant at fixed halo mass. We present a simple explanation of how feedback from active galactic nuclei (AGN) acts in our model to introduce a break in the SHM relation whose location is predicted to evolve only modestly. Finally, we show that if modifications are introduced into the model such that, for example, the gas reincorporation efficiency is no longer constant, the median SHM relation is predicted to evolve significantly over $0 < z < 4$. Specifically, we consider modifications that allow the model to better reproduce either the evolution of the stellar mass function or the evolution of average star formation rates inferred from observations.

Key words: galaxies: evolution – galaxies: formation – galaxies: haloes – galaxies: stellar content.

1 INTRODUCTION

Over the last decade, interest has grown in using statistical inference to construct empirical models that describe how galaxies are distributed within dark matter haloes (e.g. Peacock & Smith 2000; Scoccimarro et al. 2001; Berlind & Weinberg 2002; Vale & Ostriker 2004; Wang et al. 2013; Lu et al. 2014a). Observational constraints for these models typically include a selection of measurements of the abundances, clustering and lensing of galaxies, which are then combined with theoretical predictions for the abundance and clustering of dark matter haloes. Earlier work in this area typically used galaxy abundances and/or clustering as a function of luminosity to constrain model parameters (e.g. Berlind & Weinberg 2002; Yang, Mo & van den Bosch 2003; Conroy, Wechsler & Kravtsov 2006). As multiwavelength galaxy surveys have become available, it has become commonplace to replace galaxy luminosity with stellar mass (which can be estimated from broad-band photometry) as the dependent variable in this type of analysis (e.g. Mandelbaum et al. 2006; Behroozi, Conroy & Wechsler 2010; Guo et al. 2010; Moster et al. 2010). It has also become possible to place constraints on the relationship between galaxies and haloes for redshifts up to $z = 1$ and beyond (e.g. Wake et al. 2011; Behroozi, Wechsler & Conroy 2013b; Moster, Naab & White 2013; Shankar et al. 2014; Velander et al. 2014; Durkalec et al. 2015; McCracken et al. 2015).

A strong consensus that has emerged from studies of this type is that the dependence of median galaxy stellar mass, $M_\star$, on halo mass, $M_{\rm H}$, (hereafter referred to as the SHM relation) can be simply described by two power laws that connect at a stellar mass that corresponds roughly to the knee of the stellar mass function (e.g. Moster et al. 2010; Yang et al. 2012). While more complex parametrizations have been advocated (e.g. Behroozi et al. 2010, 2013b), the basic picture is that there are two regimes (the two power laws) that describe how the relative efficiency[1] of stellar mass assembly,[2] $M_\star/M_{\rm H}$, drops away either side of a peak value at the halo mass where the two power laws meet. An illustration of the relationship between the halo mass function, the stellar mass function and the median stellar mass versus halo mass (SHM) relation is shown in Fig. 1.

Arguably, a weaker level of consensus has been achieved regarding the amount of evolution in the median SHM relation that is implied by observational data. For example, Behroozi et al. (2013b)

[1] We will refer to $M_\star/M_{\rm H}$ as an 'efficiency', even though more correctly this is given by $M_\star/(f_{\rm B}M_{\rm H})$, where $f_{\rm B}$ is the universal baryon fraction.

[2] We use the convention that stellar mass assembly refers to both star formation within a galaxy and to stellar mass brought in by galaxy mergers.

* E-mail: peter.mitchell@durham.ac.uk

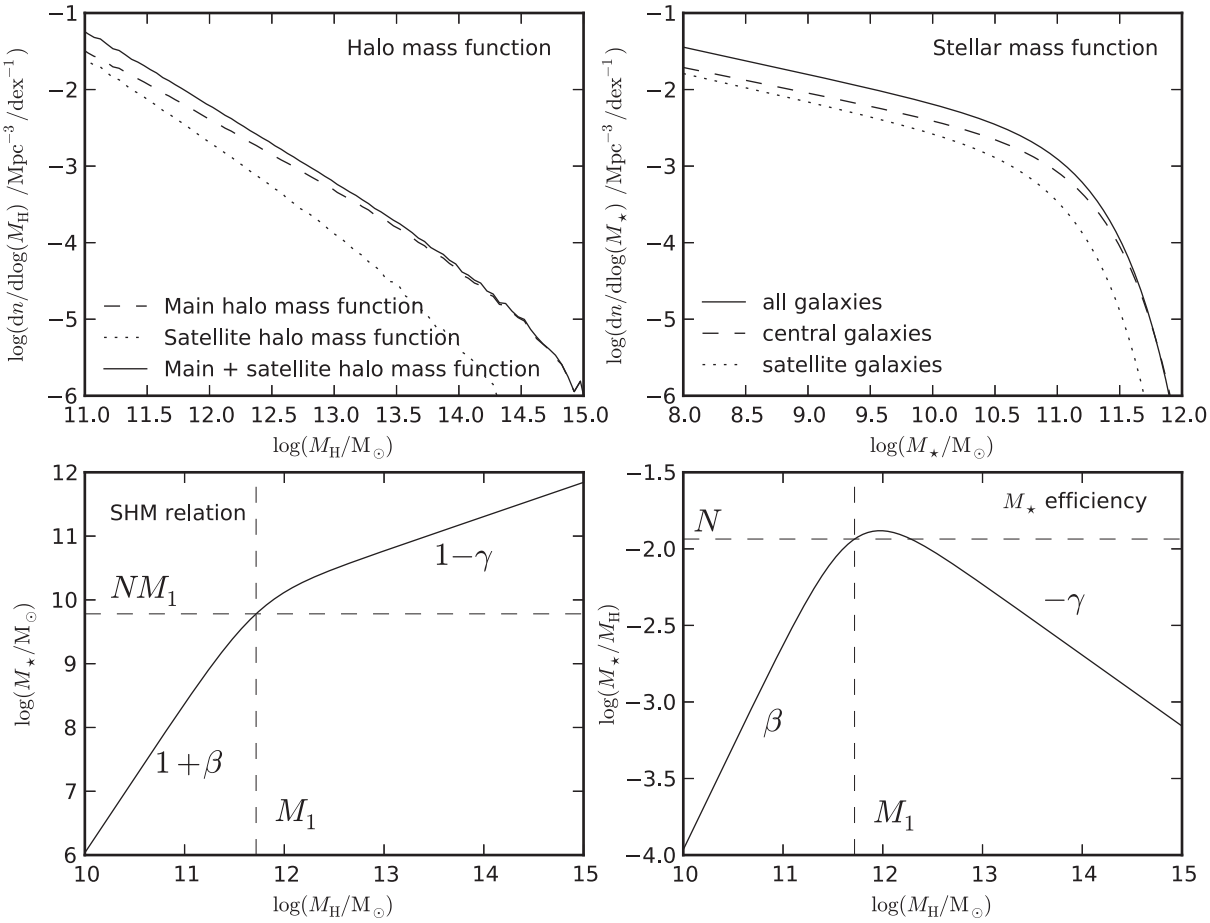

Figure 1. Schematic (based on the reference model detailed in Section 2) to demonstrate the relationship at $z = 0$ between the halo mass function, the stellar mass function and the median SHM relation. The meanings of the parameters from equation (8) are also illustrated. For example, in the lower right panel, the dashed vertical line shows the SHM break mass, M_1, and the dashed horizontal line shows the SHM normalization, N. β and $-\gamma$ are the power-law slopes shown below and above the SHM break, respectively. Upper left: main halo mass function (dashed), satellite halo mass function (dotted) and combined main plus satellite halo mass function (solid). The satellite halo mass plotted is the mass of the host subhalo at infall. Upper right: stellar mass function of all galaxies (solid), central galaxies (dashed) and satellite galaxies (dotted). Lower left: SHM relation. Lower right: median stellar mass assembly efficiency, $M_\star/M_{\rm H}$, plotted as a function of halo mass.

report that the SHM relation is marginally consistent with no evolution over the range $0 < z < 6$, although their analysis prefers a solution where the SHM break halo mass evolves, peaking at $z = 2$. Their results also show little evidence for a significant variation in the peak stellar mass assembly efficiency[3] for $z < 4$. The analysis of Moster et al. (2013) instead finds significant evidence for monotonic evolution in all SHM relation parameters (including the SHM break mass) over $0 < z < 4$, and that the peak stellar mass assembly efficiency also evolves significantly over this redshift range. Over a more limited redshift range ($0.2 < z < 1$), Leauthaud et al. (2012) report that the SHM break mass increases but that the peak stellar mass assembly efficiency remains constant, consistent with Behroozi et al. (2013b). In contrast to these three studies, (Hudson et al. 2015, for $0.2 < z < 0.8$) and (McCracken et al. 2015, for $0.5 < z < 2$) report that the SHM break mass is constant over their respective redshift intervals. Hudson et al. (2015) also find that the peak stellar mass assembly efficiency does evolve significantly over $0.2 < z < 0.8$, in agreement with Moster et al. (2013).

[3] By this, we mean the maximum value of $M_\star/M_{\rm H}$.

Disagreements between different studies are not surprising for a number of reasons. One possible source of error can be attributed to uncertain stellar mass estimates which can strongly affect the inferred stellar mass function, particularly for massive galaxies (e.g. Marchesini et al. 2009; Behroozi et al. 2010; Mitchell et al. 2013). Fairly strong priors on the distribution of errors on stellar mass estimates have to be adopted when constraining SHM parameters over a wide redshift range, where it is necessary to combine different observational data sets (e.g. Behroozi et al. 2013b; Moster et al. 2013). At high redshift, inferred stellar mass functions are typically the only observational constraint available (as opposed to clustering/weak lensing). For $z > 2$, limited depth in rest-frame optical bands, as well as complicated selection functions, can make measurements of the stellar mass function at low stellar masses very challenging, although an encouraging level of consensus has been achieved in recent years (Ilbert et al. 2013; Muzzin et al. 2013b; Tomczak et al. 2014).

Another way to connect the predicted halo population to the observed stellar population is to build a physical model that couples dark matter halo merger trees with a simple set of ordinary differential equations that govern the exchange of mass, metals and angular

momentum between different discrete galaxy and halo components. These models are typically referred to as semi-analytic galaxy formation models (e.g. Cole et al. 2000; Somerville et al. 2008; Guo et al. 2011). Alternatively, modern computers make it possible to perform hydrodynamical simulations at a resolution capable of resolving galaxies on kpc scales, within a volume that samples the halo population up to medium-sized galaxy clusters (Vogelsberger et al. 2014; Schaye et al. 2015). Using either of these two modelling techniques, the stellar mass function hosted by a given halo population is predicted and can be compared against observational estimates of the stellar mass function without having to assume any parametric form for the SHM relation. In general, these modelling techniques have provided support for the parametric forms assumed in empirical studies (e.g. Zehavi, Patiri & Zheng 2012; Henriques et al. 2013).

In this paper, we analyse the predictions made using the semi-analytic model GALFORM, focusing on the evolution of the median SHM relation. Unlike other recent work using similar models, we do not attempt to find a best-fitting model to some combination of observational data (Henriques et al. 2013; Benson 2014; Lu et al. 2014b; Henriques et al. 2015). Instead, we address the questions: what type of evolution is naturally predicted by semi-analytic models for the SHM relation? How much variation in this evolution can be achieved by adjusting model parameters? What does this evolution tells us about the underlying galaxy formation physics?

Although the model analysed here is just one example of a modern semi-analytic galaxy formation model, most of our results can be regarded as fairly general predictions of the semi-analytic modelling technique (we attempt to point out any obvious exceptions to this at the appropriate points in the text). With that said, work from several groups has, in recent years, been focused on modifying traditional semi-analytic physics parametrizations[4] for star formation, supernova (SNe) feedback, and gas reincorporation in order to try to explain the myriad of observational galaxy evolution results that have been enabled by recent multiwavelength surveys (Henriques et al. 2013, 2015; Hirschmann et al. 2014; Mitchell et al. 2014; Cousin et al. 2015b; White, Somerville & Ferguson 2015). While we do not attempt to explore the breadth of predictions for the evolution of the SHM relation that would result from exploring all of the modifications that have been suggested (which in some cases are substantial), we do present a more limited analysis of the modified gas reincorporation models from our previous work on the star-forming sequence (Mitchell et al. 2014).

The layout of the paper is as follows. In Section 2, we give a brief overview of our reference model. In Section 3, we present model predictions for the evolution in the SHM relation. In Section 4, we attempt to explain these predictions in simple terms. In Section 5, we assess the impact of changing individual model parameters. In Section 6, we consider the range in SHM evolution that is displayed by a number of models that have been roughly tuned to match the local stellar mass function. We discuss and summarize our results in Sections 7 and 8, respectively. All data used to produce figures shown in this paper can be made available on request by contacting the corresponding author (an email address is provided on the first page).

[4] Which are appropriate for matching the local luminosity/stellar mass function.

2 THE GALFORM GALAXY FORMATION MODEL

In this paper, we explore the predictions for the evolution of the SHM relation made by the semi-analytic galaxy formation model, GALFORM. GALFORM is an example of a model that is built upon the halo merger trees that can be obtained from numerical simulations or analytical calculations of the hierarchical structure formation that takes place within a Λ cold dark matter (CDM) cosmological model. The basis of the model is that within each subhalo, the baryonic content of galaxies can be compartmentalized into discrete components, including disc, bulge and halo components. A set of differential equations can then be constructed that describe how baryonic mass, angular momentum and metals are exchanged between these discrete components. The various terms that appear in these continuity equations each represent the effects of a distinct physical process, such as gas cooling or star formation. A detailed overview of the original implementation of the GALFORM model can be found in Cole et al. (2000). Significant updates to the physical modelling are described in (Bower et al. 2006, active galactic nuclei – AGN feedback) and (Lagos et al. 2011, star formation law). An overview of the most recent implementation of the model can be found in Lacey et al. (2015). General introductions to semi-analytic modelling of galaxy formation can be found in Baugh (2006), Benson (2010) and Somerville & Davé (2015).

For the reference model used in this paper, we use the model presented in Gonzalez-Perez et al. (2014). This model uses merger trees extracted from the MR7 simulation (Guo et al. 2013), which represents an update of the MILLENNIUM simulation (Springel et al. 2005), using *Wilkinson Microwave Anisotropy Probe* (*WMAP*)-7 cosmological parameters (Komatsu et al. 2011). As such, unless specified otherwise, we assume the following cosmological parameters: $\Omega_{\rm m} = 0.28$, $\Omega_\Lambda = 0.728$, $\Omega_{\rm b} = 0.045$, $\sigma_8 = 0.81$ and $h = 0.704$.

The parameters of the Gonzalez-Perez et al. (2014) model were explicitly tuned to reproduce the observed $b_{\rm J}$ and K-band luminosity functions at $z = 0$, while also giving reasonable evolution compared to the observed rest-frame UV and K-band luminosity functions. It should be noted that the model was not tuned to reproduce the local stellar mass function inferred from observations. A comparison between our reference model and observational estimates of the local stellar mass function can be seen in the top-left panel of Fig. 7. Compared to observational estimates, the model underpredicts the abundance of galaxies at and around the knee of the stellar mass function. Note that in this paper, model predictions for the stellar mass function are always shown using the intrinsic stellar masses from the model (so no attempt is made to replicate the effects of random or systematic measurement error in stellar mass estimates).

For all results presented in this paper, we use corrected DHalo masses to represent the masses of dark matter haloes (Jiang et al. 2014). DHalo masses are defined as the sum of the masses of the subhaloes that the DHalo algorithm associates with a given DHalo. The mass of each subhalo is defined as the sum of the masses of the particles that are determined to be gravitationally bound to the subhalo by the SUBFIND algorithm (Springel et al. 2001).[5] DHalo masses are then corrected (in some cases) to ensure mass conservation such that all haloes grow monotonically in mass in the

[5] Note that the DHalo mass definition is therefore not equivalent to other commonly used halo mass definitions such as M_{200} (the mass enclosed within a sphere that has a mean density that is 200 times the critical density of the Universe).

merger trees. When quoting halo masses for central galaxies, the halo mass quoted is the corresponding DHalo mass. For satellite galaxies, the halo mass quoted is the maximum past DHalo mass of the hosting subhalo. Subhaloes are identified as satellites (for the first time) by the DHalo algorithm if they are enclosed within twice the half-mass radius of a more massive subhalo and they have lost at least 25 per cent of their past maximum mass (see appendix A3 in Jiang et al. 2014).

The DHalo halo mass definition is similar to but not the same as the conventions followed by the abundance matching studies which we compare against later in this paper (Behroozi et al. 2013b; Moster et al. 2013). Furthermore, there are significant differences in the abundance of satellite galaxies between our model and the empirical models of Behroozi et al. (2013b) and Moster et al. (2013). In Appendix A, we present an analysis of this issue, along with details of a method to correct for the resultant differences in halo catalogues when comparing predictions for the SHM relation from our model with the results of abundance matching. When showing results from abundance matching for the evolution of the SHM relation, we show both the evolution taken directly from Behroozi et al. (2013b) and Moster et al. (2013) and the corresponding evolution we find after applying this correction.

2.1 Implementation of star formation, SNe feedback and gas reincorporation

Before presenting our results, it is useful to review the basic physical processes that regulate the rate ($\dot{M}_\star$) and efficiency ($\dot{M}_\star/\dot{M}_{\rm H}$) of stellar mass assembly for actively star-forming galaxies in our model. For star-forming galaxies, where radiative cooling time-scales are typically short and AGN feedback is ineffective, the relevant parts of the model that control the rate and efficiency of stellar mass assembly are the cosmological infall rate, the star formation law, the efficiency of SNe feedback and the time-scale over which the ejected gas is reincorporated into the gas halo.

Assuming gas traces dark matter accretion rates on to haloes, specific gas accretion rates, on average, scale strongly with redshift, approximately as $\dot{M}_{\rm g}/M_{\rm g} \propto (1+z)H(z)$ in the ΛCDM model (Fakhouri, Ma & Boylan-Kolchin 2010). Once gas is accreted on to a given halo, it takes approximately a single halo dynamical time to freefall[6] on to the disc at the centre of the halo. The halo dynamical time, $t_{\rm dyn}$ is defined as

$$t_{\rm dyn} \equiv \frac{r_{\rm H}}{V_{\rm H}} = \frac{G M_{\rm H}}{V_{\rm H}^3}, \tag{1}$$

where $r_{\rm H}$ is the halo virial radius, $V_{\rm H}$ is the halo circular velocity at that radius, $M_{\rm H}$ is the halo mass and G is the gravitational constant.

As introduced in Lagos et al. (2011), cold gas in galaxy discs is turned into stars at a rate given by the empirical Blitz & Rosolowsky (2006) molecular gas star formation law,

$$\Sigma_{\rm SFR} = \nu_{\rm SF} f_{\rm mol} \Sigma_{\rm gas}, \tag{2}$$

where $\Sigma_{\rm SFR}$ is the star formation rate surface density, $\nu_{\rm SF}$ is the inverse of a characteristic star formation time-scale, $f_{\rm mol}$ is the fraction of cold hydrogen gas in the molecular phase and $\Sigma_{\rm gas}$ is the total cold gas surface density. Equation (2) is integrated over the surface of the disc to obtain the star formation rate, ψ. By assuming instantaneous recycling in stellar evolution, the rate of change of stellar mass in the disc is related to ψ by

$$\dot{M}_\star = (1-R)\psi, \tag{3}$$

where R is the fraction of mass returned to the cold ISM through stellar evolution.

As cold gas forms stars in a disc, a fraction of the cold gas reservoir is continuously ejected from the disc, representing the effects of SNe feedback. This is quantified by the dimensionless mass loading factor, $\beta_{\rm ml}$, which is parametrized as a function of the disc circular velocity at the half-mass radius, $V_{\rm disc}$, such that

$$\beta_{\rm ml} = (V_{\rm disc}/V_{\rm hot})^{-\alpha_{\rm hot}}, \tag{4}$$

where $V_{\rm hot}$ and $\alpha_{\rm hot}$ are model parameters. The outflow rate from the disc is related to $\beta_{\rm ml}$ by

$$\dot{M}_{\rm ej} = \beta_{\rm ml}\,\psi. \tag{5}$$

The effective gas depletion time-scale of a galaxy disc, $t_{\rm eff}$ is therefore given by

$$t_{\rm eff} = \frac{M_{\rm cold}}{\psi(1-R+\beta_{\rm ml})}, \tag{6}$$

where $M_{\rm cold}$ is the cold gas mass in the disc.

All of the gas that is ejected from a galaxy disc by SNe feedback is then added to a reservoir, $M_{\rm res}$, of ejected gas which, in turn, is reincorporated back into the gas halo at a rate, $\dot{M}_{\rm ret}$, given by

$$\dot{M}_{\rm ret} = \frac{\alpha_{\rm reheat} M_{\rm res}}{t_{\rm dyn}}, \tag{7}$$

where $\alpha_{\rm reheat}$ is a model parameter. In our reference model, $\alpha_{\rm reheat} = 1.26$, such that ejected gas is reincorporated back into the halo roughly over a halo dynamical time-scale.

To summarize, gas is accreted from the halo on to the disc over roughly a halo dynamical time-scale, $t_{\rm dyn}$. Cold gas is depleted from the disc over an effective disc depletion time-scale, $t_{\rm eff}$. Given the model parameters, the majority of this cold gas is ejected and subsequently reincorporated into the halo over roughly a halo dynamical time-scale, $t_{\rm dyn}$. It is important to note that for the haloes hosting star-forming galaxies in our reference model, SNe feedback is very strong, such that $\beta_{\rm ml}$ typically significantly exceeds unity. As a result, $t_{\rm eff}$ tends to be much shorter than the other relevant time-scale of the system ($t_{\rm dyn}$). In this regime, the star formation law adopted in our model (given by equation 2) has minimal impact on the efficiency of stellar mass assembly. Instead, the efficiency is governed by the mass loading factor, $\beta_{\rm ml}$ and the number of times gas can be cycled by feedback through a halo after being accreted ($\approx t_{\rm H}/2t_{\rm dyn} \approx 5$). We refer the interested reader to section 4.2 in Mitchell et al. (2014) for a more detailed discussion of this point.

3 THE PREDICTED EVOLUTION IN THE SHM RELATION

In Fig. 2, we show the evolution in the SHM distribution of our reference model. For this paper, we are primarily interested in understanding the evolution of the median SHM relation, as opposed to the complete SHM distribution. We note however that our reference model does not predict that the intrinsic scatter around the median SHM relationship is strictly lognormal with constant width. This is in contrast to what is assumed in various abundance matching studies (Yang et al. 2012; Behroozi et al. 2013b; Moster et al. 2013). We explore this topic further in Appendix B.

[6] Radiative cooling time-scales are almost always shorter than the gravitational freefall time for haloes that host actively star-forming galaxies.

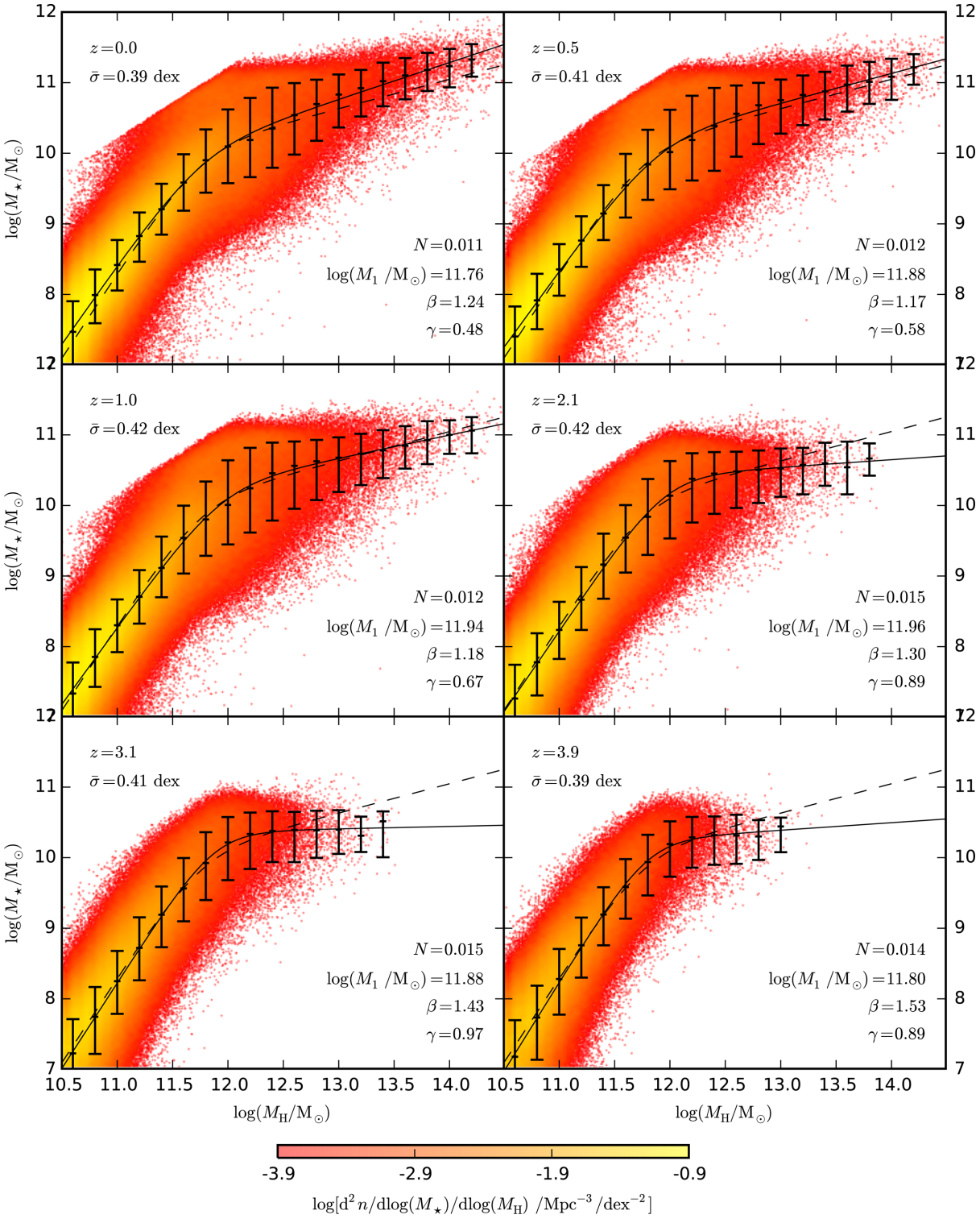

Figure 2. Stellar mass plotted as a function of halo mass in our reference model. Each panel corresponds to a different redshift, as labelled. The coloured points represent individual model galaxies and the point colours are scaled with the logarithm of the local point density. The corresponding number densities are indicated by the colour bar at the bottom of the figure. The black points and associated error bars show the median, 16$^{\rm th}$ and 84$^{\rm th}$ percentiles of the distribution at a given halo mass. $\bar{\sigma}$ quantifies the mean scatter in stellar mass within bins of halo mass above $\log(M_{\rm H}/{\rm M}_{\odot}) = 10.5$. The scatter in each bin is defined as half of the central 68 per cent range in $\log(M_{\star})$. Black solid lines show the parametrization given in equation (8), fit to the medians of the distribution. The values of N, M_1, β and γ shown in each panel are the best-fitting parameters from this parametrization. Black dashed lines show a similar fit but with the constraint that the fitting parameters do not evolve with redshift. Each redshift shown is assigned equal weight in the fit. The best-fitting parameters for this fit are $N = 0.012$, $\log(M_1/{\rm M}_{\odot}) = 11.75$, $\beta = 1.41$ and $\gamma = 0.59$.

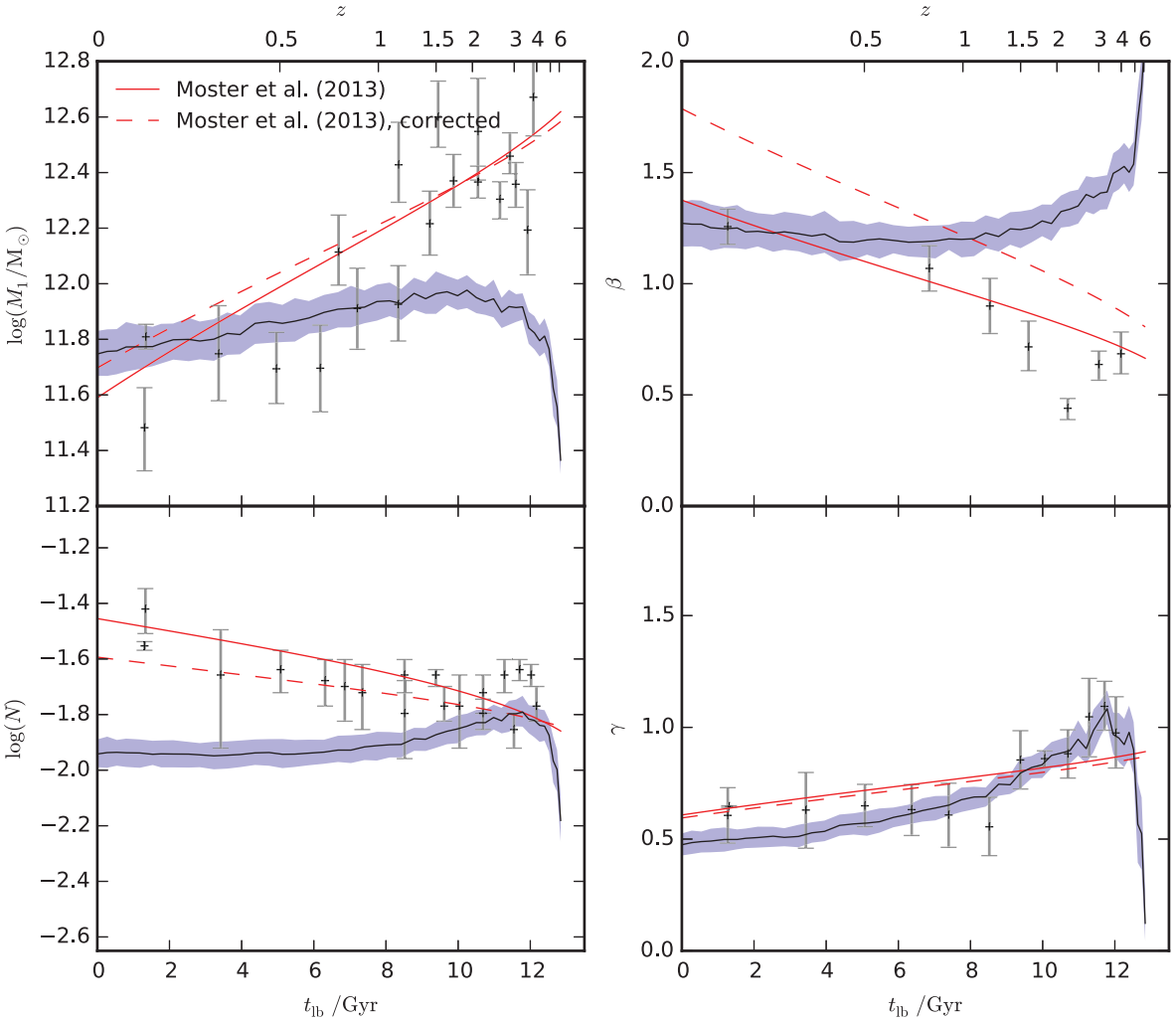

Figure 3. Evolution in the fitting parameters for the median relationship between stellar mass and halo mass predicted in our reference model (see equation 8). Black solid lines show the median of the projected posterior distribution for each parameter. Blue shaded regions show the 16$^{\rm th}$ to 84$^{\rm th}$ percentile range of the posterior distributions. Red solid lines show the best-fitting parametric evolution determined by Moster et al. (2013) using multi-epoch abundance matching. Grey points show the associated best-fitting SHM parameters and 1σ error bars determined by Moster et al. (2013) using single epoch abundance matching applied to individual stellar mass functions from the literature. Red dashed lines show the best-fitting parametric evolution we obtain after correcting the Moster et al. (2013) SHM relation to be compatible with the halo catalogues used in GALFORM.

To quantify the evolution in the median SHM relation, we adopt the parametrization of Moster et al. (2013), which relates the median stellar mass at a given halo mass to halo mass by

$$\frac{M_\star}{M_{\rm H}} = 2\,N\left[\left(\frac{M_{\rm H}}{M_1}\right)^{-\beta} + \left(\frac{M_{\rm H}}{M_1}\right)^{\gamma}\right]^{-1}, \qquad (8)$$

where N is a parameter controlling the normalization, M_1 controls the position of the break,[7] β sets the power-law slope below the break and γ sets the slope above it. The meaning of each parameter can be seen in Fig. 1.

The evolution in these parameters is shown in Fig. 3, along with abundance matching results from Moster et al. (2013) for comparison. We show (solid red lines) the evolution in SHM parameters using the best-fitting parametric evolution from table 1 in Moster et al. (2013), which were inferred from observational stellar mass function data from Baldry, Glazebrook & Driver (2008), Pérez-González et al. (2008), Li & White (2009) and Santini et al. (2012). We also show (dashed red lines) the evolution of SHM fitting parameters which we obtain after correcting for the differences in input halo catalogues between our reference GALFORM model and Moster et al. (2013). In effect, this shows the SHM fitting parameters that Moster et al. (2013) would have obtained, had they used our definition of halo mass and our treatment of satellite galaxies (and their associated subhaloes). The method used to calculate this correction is described in Appendix A.

Compared to the results from Moster et al. (2013), our reference model predicts modest evolution in most of the SHM parameters. In particular, the 1σ posterior distributions for β, M_1 and N are consistent with there being no evolution in these parameters for $z < 4$. This is in contrast to the observational abundance matching results, which suggest comparatively strong evolution in β and M_1 over the same redshift range. By comparing solid and dashed red lines, it appears that this difference between our model and

[7] Note that M_1 is closely related to (but not exactly equal to) the characteristic halo mass corresponding to peak stellar mass assembly efficiency (the maximum value of $M_\star/M_{\rm H}$).

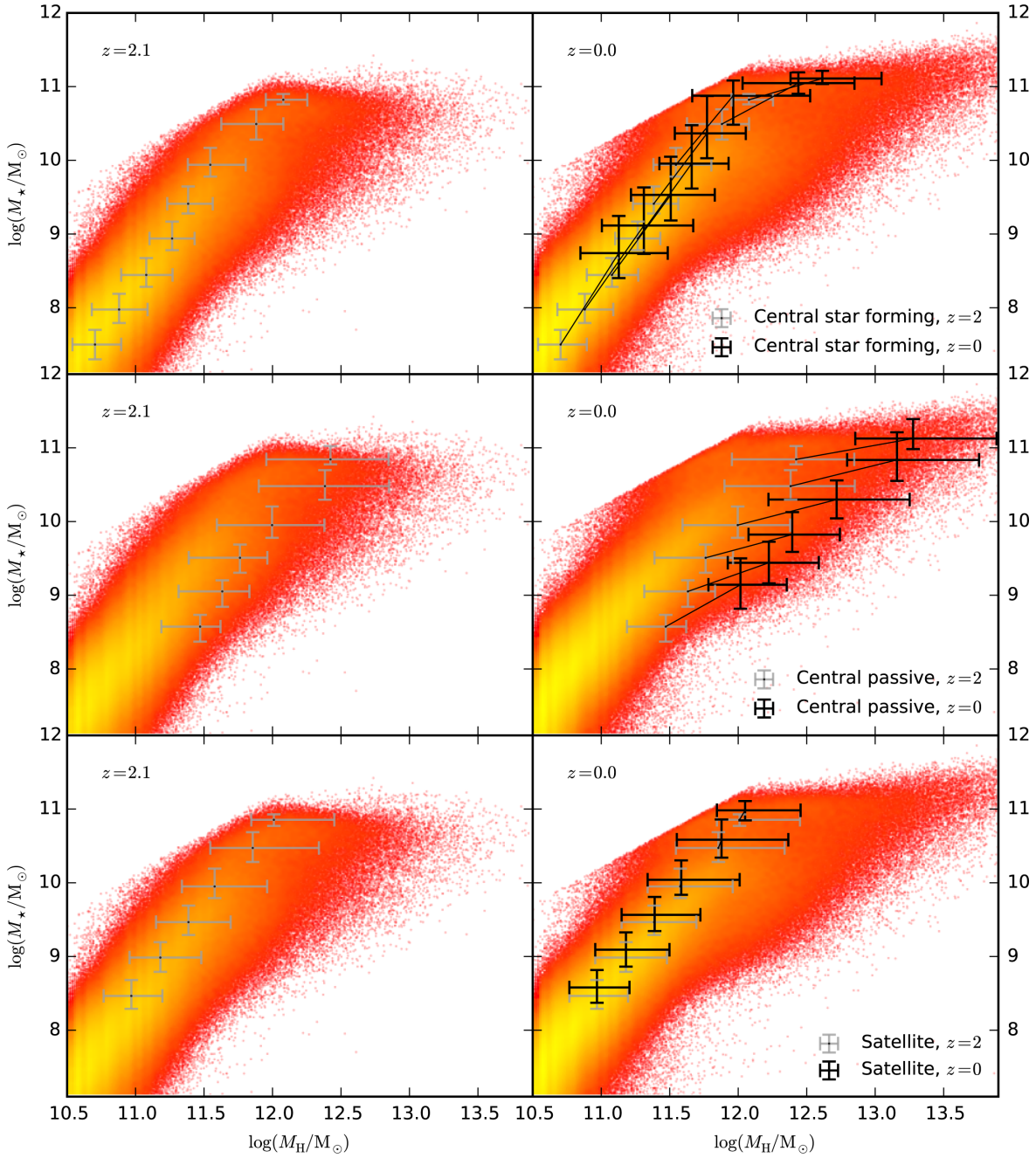

Figure 4. Evolution of populations of galaxies across the SHM plane in our reference model. In all panels, the coloured points show the distribution for the entire galaxy population at the redshift labelled at the top-left corner of each panel. Subpopulations of galaxies are selected in stellar mass bins at $z = 2$ (grey error bars). Each subpopulation is then tracked to $z = 0$ (black error bars) and the intervening evolution of each subpopulation is then indicated by solid black lines connecting grey and black error bars. Top: evolution of central star-forming galaxies. These are galaxies that are star forming for at least 90 per cent of the simulation outputs between $z = 2$ and 0. Middle: evolution of central passive galaxies. These are central galaxies that are star forming before $z \sim 2$ but are then passive after $z \sim 2$. Bottom: evolution of satellite galaxies. These are galaxies that are central before $z \sim 2$ that then become satellites after $z \sim 2$. The error bars show the 10^{th} and 90^{th} percentiles in both stellar mass and halo mass for each subpopulation and stellar mass bin.

abundance matching is robust against differences in the input halo catalogues. This demonstrates that there are differences between our reference model and the Moster et al. (2013) empirical model that are caused instead by the details of the implementation of baryonic physics in our reference model.

To try to understand the reasons for the modest evolution in the SHM relation predicted by our reference model, we split the overall population into subsamples of central star-forming, central passive and satellite galaxies. To split star forming from passive galaxies, we use the same evolving cut in specific star formation rate against stellar mass that was used in Mitchell et al. (2014).[8] The evolution in the SHM relations for these subsamples is shown in Fig. 4. Starting

[8] The analytic evolution of the cut is designed by hand to separate the distributions of star-forming and passive galaxies at all redshifts considered.

with central star-forming galaxies, in the top panels of Fig. 4 we show how a sample of model star-forming galaxies has evolved since $z = 2$. Specifically, we select central galaxies that are classed as star forming for at least 90 per cent of the output times in our merger trees between $z = 2$ and 0. Fig. 4 shows directly that these model galaxies essentially evolve along an invariant power law in the $M_\star$ versus $M_{\rm H}$ plane. This power law is consistent with the overall SHM relation below the break mass (M_1), explaining why the overall SHM relation does not evolve significantly in this halo mass range. We note that this phenomenon has also been inferred from observational weak lensing data between $z = 1$ and 0 by Hudson et al. (2015). This behaviour is, however, broken in the two highest stellar mass bins (spanning $10.25 < \log(M_\star\,{\rm M}_\odot) < 11.25$) of central star-forming galaxies selected at $z = 2$. Here, the fractional growth in stellar mass is outpaced by the fractional growth of dark matter haloes.

In the middle panels of Fig. 4, we show a sample of central model galaxies that are star forming before $z = 2$ and then become passive at $z < 2$. Specifically, we select galaxies that are star forming for >90 per cent of the simulation output times for $z > 2$ and are passive for >90 per cent of the simulation output times for $z < 2$. By $z = 0$, these galaxies are displaced from the median of the SHM distribution for star-forming galaxies, preferentially residing in more massive haloes at a given stellar mass. It is apparent that these passive galaxies do not follow the same evolutionary path of all but the most massive star-forming galaxies shown in Fig. 4. Instead, the growth in their host dark matter haloes outpaces any stellar mass assembly through galaxy mergers. This behaviour helps to create the break in the overall SHM relation above $M_{\rm H} = M_1$, where passive central galaxies dominate the overall population.

Finally, for completeness, in the bottom panels of Fig. 4 we show a sample of model galaxies that are central before $z = 2$ and then become satellites after $z = 2$. Specifically, we select galaxies that are central for >90 per cent of the simulation output times before $z = 2$ and are satellites for >90 per cent of the simulation output times for $z < 2$. Fig. 4 shows the expected result that our model predicts that satellite galaxies do not grow significantly in stellar mass after infall. This result is expected because of the implementation of hot gas stripping and SNe feedback in this version of GALFORM.[9] By definition, for the SHM relation, satellite halo masses are set as the mass of the associated subhalo at infall. Without any significant star formation activity after infall, satellites therefore simply remain frozen in place in the SHM plane. As the SHM relation below the break does not evolve significantly in our reference model, satellites do not become significantly displaced from the total SHM distribution after infall.

We note that the instantaneous hot gas stripping used in our reference model is unlikely to be realistic (Font et al. 2008; Henriques et al. 2015). Observational data suggest that satellite galaxies typically continue to form stars at a comparable rate to central galaxies for a significant length of time after infall (e.g. Peng et al. 2010; Wetzel, Tinker & Conroy 2012; Wetzel et al. 2013; McGee, Bower & Balogh 2014). However, based on results from Watson & Conroy (2013), who use galaxy clustering and group catalogues to show that the SHM relation for satellite galaxies is consistent with the SHM relation for central galaxies over $0 < z < 2$, we do not expect that the abrupt quenching of satellite galaxies after infall in our model will adversely affect predictions for the median SHM relation.

[9] Hot gas is instantaneously stripped from satellite haloes and strong SNe feedback typically ejects the majority of the cold gas on a short time-scale.

4 PHYSICAL REASONS FOR THE LACK OF EVOLUTION IN THE PREDICTED SHM RELATION

In Section 3, we showed that our reference model predicts that, below a break halo mass, M_1, the median SHM relationship does not evolve significantly over $0 < z < 4$. In this section, we attempt to explain, in simple terms, why our reference model predicts minimal evolution in the SHM relation below M_1, the origin of the break mass, M_1, and why the predicted high-mass slope of the SHM relation above the break increases with cosmic time. To do so, we consider the impact of SNe feedback, AGN feedback and galaxy mergers on the SHM relation predicted by our reference model. For reasons of clarity, we introduce (for this section only) two new variables, $\beta' \equiv 1 + \beta$ and $\gamma' \equiv 1 - \gamma$ (where β and γ are parameters from the fitting formula given by equation 8). β' and γ' are the power slopes of the SHM relation such that $M_\star \propto M_{\rm H}^{\beta'}$ for $M_{\rm H} \ll M_1$ and $M_\star \propto M_{\rm H}^{\gamma'}$ for $M_{\rm H} \gg M_1$.

4.1 Star-forming galaxies

Below a break halo mass, M_1, Fig. 3 shows that our reference model does not predict significant evolution in the SHM relation over $0 < z < 4$. For halo masses below M_1, the galaxy population in our model is dominated by central star-forming and satellite galaxies (as opposed to central passive galaxies). In this halo mass regime, the median SHM relation is well described by a non-evolving power law with slope $\beta' = 1 + \beta \approx 2.3$ for $z < 4$. This is interesting, given that for star-forming galaxies, it might be expected in the simplest possible case that the star formation rate, $\dot{M}_\star$, would simply track the accretion rate on to haloes, $\dot{M}_{\rm H}$. In this case, individual galaxies would evolve along a power law in the SHM plane with slope, $\beta' = 1$. To evolve along a power law where $\beta' \approx 2.3$ requires instead that

$$\dot{M}_\star \propto M_{\rm H}^{1.3}\dot{M}_{\rm H}, \tag{9}$$

implying that stellar mass assembly increases in efficiency as the host haloes grow in mass. It should be noted that this also requires that at fixed halo mass, the instantaneous star formation efficiency,

$$\eta_{\rm SF} \equiv \dot{M}_\star/(f_{\rm B}\dot{M}_{\rm H}), \tag{10}$$

is constant across cosmic time (here, $f_{\rm B}$ is the cosmic baryon fraction). In Mitchell et al. (2014), we showed that $\eta_{\rm SF}$ does evolve for populations of star-forming galaxies in GALFORM as their haloes grow in mass. This occurs predominantly because of evolution in the mass loading factor for SNe feedback,[10] $\beta_{\rm ml}$, although a small amount of evolution in the gas reincorporation efficiency also contributes (Mitchell et al. 2014).

[10] We note that for some of the discussion presented in Mitchell et al. (2014), we further simplified this picture by assuming that $\beta_{\rm ml}$ is constant over some redshift range, which results in $\dot{M}_\star/M_\star \propto \dot{M}_{\rm H}/M_{\rm H}$. While this is approximately true at lower redshifts, it is an oversimplification when considering the evolution of the SHM relation.

In GALFORM, $\beta_{\rm ml} \propto V_{\rm disc}^{-\alpha_{\rm hot}}$, where $V_{\rm disc}$ is the disc circular velocity at the half-mass radius. Roughly speaking, the disc circular velocity scales with the halo circular velocity, $V_{\rm H}$, in smaller haloes where baryon self-gravity effects are not important. These are the haloes that typically host star-forming galaxies and also the haloes where SNe feedback plays the largest role in regulating star formation rates. Again, roughly speaking,[11] it is expected that the instantaneous star formation efficiency, $\eta_{\rm SF}$, will scale with $(1+\beta_{\rm ml})^{-1} \approx \beta_{\rm ml}^{-1}$ (Mitchell et al. 2014). Therefore, it is to be expected that in low-mass haloes that host star-forming galaxies,

$$\eta_{\rm SF} \propto \beta_{\rm ml}^{-1} \propto V_{\rm disc}^{\alpha_{\rm hot}} \propto V_{\rm H}^{\alpha_{\rm hot}} \propto M_{\rm H}^{\alpha_{\rm hot}/3}\, \bar{\rho}_{\rm H}^{\alpha_{\rm hot}/6}, \tag{11}$$

where $\bar{\rho}_{\rm H}$ is the mean halo density, which is related to $V_{\rm H}$ through

$$\bar{\rho}_{\rm H} = \frac{3M_{\rm H}}{4\pi R_{\rm H}^3}, \quad V_{\rm H}^2 = \frac{GM_{\rm H}}{R_{\rm H}}. \tag{12}$$

$\bar{\rho}_{\rm H}$ is independent of halo mass, but does instead depend on the expansion factor, a, through

$$\bar{\rho}_{\rm H} = \Delta_{\rm vir}(a)\rho_{\rm crit}(a), \tag{13}$$

where $\Delta_{\rm vir}(a)$ is the overdensity of collapsed haloes relative to the critical density and $\rho_{\rm crit}(a)$ is the critical density of the Universe.

If we make the approximation that the rate of halo mass growth outpaces halo density growth, such that $\bar{\rho}_{\rm H}$ is effectively constant over the time-scale for haloes to assemble their mass, then straightforward integration of equation (11) yields

$$M_\star \propto M_{\rm H}^{1+\alpha_{\rm hot}/3}, \tag{14}$$

which, for the value of $\alpha_{\rm hot} = 3.2$ used in our reference model, yields $M_\star \propto M_{\rm H}^{2.07}$. This implies $\beta' = 2.07$, close to the value, $\beta' = 2.3$ predicted by our reference model. Therefore, we see that the slope of the SHM relation primarily reflects the exponent, $\alpha_{\rm hot}$, in the SNe feedback mass loading parametrization. We note that the mean halo density, $\bar{\rho}_{\rm H}$, is not constant across cosmic time. However, in Appendix C we explain why this is not a bad approximation when integrating equation (11). We show that for $z > 1$, halo mass accretion rates greatly outpace the rate of change in $\bar{\rho}_{\rm H}$. Another important effect is that, on average, halo densities evolve more slowly for haloes in GALFORM when compared to the spherical collapse model. This is because halo circular velocities (and hence mean halo densities at fixed halo mass) in our reference model are only updated to match the spherical collapse model when haloes double in mass. This effect is particularly important for $z < 1$ when halo mass doubling events are infrequent (as halo mass accretion rates have decreased compared to high redshift).

4.2 AGN feedback

We now consider the origin of the break halo mass, M_1, which marks the point above which the efficiency of stellar mass assembly drops with respect to the efficiency of halo mass assembly. Moreover, we seek to explain why M_1 does not evolve significantly in our model for $z < 4$ (see Fig. 3).

In our model, the efficiency of stellar mass assembly drops in massive, quasi-hydrostatic haloes because AGN feedback acts to shut down cooling from hot gas coronae on to the central galaxy. For the AGN feedback model implemented in GALFORM, the primary requirement for AGN feedback to be effective in suppressing cooling is that a halo is in quasi-hydrostatic equilibrium, which is taken to be true if

$$t_{\rm cool}(r_{\rm cool}) > \alpha_{\rm cool}^{-1}\, t_{\rm ff}(r_{\rm cool}), \tag{15}$$

where $t_{\rm cool}$ is the radiative cooling time-scale evaluated at a radius $r_{\rm cool}$, $\alpha_{\rm cool}$ is a model parameter and $t_{\rm ff}$ is the gravitational freefall time-scale evaluated at $r_{\rm cool}$ in (Navarro, Frenk & White 1997; NFW) halo. The cooling radius $r_{\rm cool}$ is defined as the radius below which the enclosed gas had sufficient time to cool through radiative processes since the previous halo formation event (Cole et al. 2000).

On average, equation (15) sets a threshold halo mass above which AGN feedback is effective. A simplified expectation for how this AGN feedback threshold mass evolves with time can be obtained by evaluating $t_{\rm cool}$ at the mean gas density within the halo, $\bar{\rho}_{\rm g}$,

$$t_{\rm cool}(\rho_{\rm g} = \bar{\rho}_{\rm g}) = \frac{3}{2}\frac{k_{\rm B}T}{\mu m_{\rm p}}\frac{1}{\bar{\rho}_{\rm g}\Lambda(Z_{\rm g}, T)}, \tag{16}$$

where $\Lambda(Z_{\rm g}, T)$ is the cooling function, which depends on the hot gas metallicity, $Z_{\rm g}$, and temperature, T, evaluated at the mean gas density. Assuming the gas temperature is equal to the virial temperature of the halo, $T_{\rm vir}$, given by

$$T_{\rm vir} = \frac{1}{2}\frac{\mu m_{\rm p}}{k_{\rm B}} V_{\rm H}^2, \tag{17}$$

we obtain the scaling that

$$t_{\rm cool} \propto \frac{V_{\rm H}^2}{\bar{\rho}_{\rm g}\Lambda(T,Z)} \propto \frac{V_{\rm H}^2}{\bar{\rho}_{\rm H}\Lambda(T,Z)} \propto \frac{M_{\rm H}^{2/3}}{\bar{\rho}_{\rm H}^{2/3}}\frac{1}{\Lambda(T,Z)}. \tag{18}$$

For a fixed NFW halo concentration, the freefall time-scales with the halo dynamical time-scale, $t_{\rm dyn} = GM_{\rm H}/V_{\rm H}^3$, such that

$$t_{\rm ff} \propto t_{\rm dyn} \propto \frac{M_{\rm H}}{V_{\rm H}^3} \propto \bar{\rho}_{\rm H}^{-1/2}. \tag{19}$$

We can then evaluate equation (15) for $t_{\rm cool} = t_{\rm ff}$, yielding a threshold halo mass for effective AGN feedback that evolves according to

$$\frac{M_{\rm H}^{2/3}}{\bar{\rho}_{\rm H}^{2/3}}\frac{1}{\Lambda(T,Z)} \propto \bar{\rho}_{\rm H}^{-1/2}, \tag{20}$$

which implies that

$$M_{\rm H} \propto \Lambda(T,Z)^{3/2}\bar{\rho}_{\rm H}^{1/4} \propto \Lambda(T,Z)^{3/2}\,[\Delta_{\rm c}(a)\rho_{\rm crit}(a)]^{1/4}. \tag{21}$$

In other words, we expect AGN feedback to suppress cooling (and therefore star formation) above a characteristic halo mass which is only weakly dependent on redshift ($M_{\rm H} \propto [\Delta_{\rm c}(a)\bar{\rho}(a)]^{1/4}$), for a fixed hot gas metallicity and temperature. This simple expectation is qualitatively consistent with the modest evolution in the SHM break mass predicted in our reference model. A more detailed exploration of the behaviour of AGN feedback in our model is presented in Appendix D. We also refer the interested reader to the discussion presented in section 6.6 of Leauthaud et al. (2012) on whether the efficiency of stellar mass assembly efficiency actually peaks at a given $M_\star/M_{\rm H}$ ratio, rather than at fixed halo mass, as we have described here.

4.3 Mergers

Finally, we give brief consideration to the evolution of the high-mass SHM slope, γ', which is predicted to evolve from $\gamma' \approx 0$ at $z = 4$ to

[11] This is not a precise statement because finite gas reincorporation and freefall/radiative cooling time-scales will cause the full effects of any instantaneous changes in $\beta_{\rm ml}$ to take time to propagate through the system of equations.

Table 1. Description of the model parameters that are varied in Section 5 to produce the set of models shown in Figs 5 and 6. In all cases, the reference model is the intermediate model for the quoted parameter values.

$V_{\rm hot}$	133, 425, 600 km s^{-1}	Normalization of SNe feedback. Change such that the mass loading factor, $\beta_{\rm ml}$, changes up or down by a factor of 3.
$\alpha_{\rm hot}$	1.6, 3.2, 4.8	Dependence of SNe feedback on galaxy circular velocity. Change up or down by $\pm$50 per cent. Also change $V_{\rm hot}$ such that $\beta_{\rm ml}$ is fixed for a circular velocity, $V_{\rm disc} = 200$ km s^{-1}.
$\alpha_{\rm reheat}$	0.42, 1.26, 3.78	Ejected gas reincorporation rate. Change such that $1 + 2\pi\alpha_{\rm reheat}$ changes up or down by a factor of 3. This factor corresponds to the approximate reincorporation efficiency, given by equation (22) in Mitchell et al. (2014).
$\nu_{\rm sf}$	0.17, 0.5, 1.7 Gyr^{-1}	Disc SF law normalization.
$\alpha_{\rm cool}$	0.2, 0.6, 1.8	AGN feedback cooling suppression threshold.
$\eta_{\rm disc}$	0.61, 0.8, 2.4	Disc instability threshold. Change up by a factor of 3 and down to 0.61 (minimum value below which all discs are stable).
$f_{\rm dyn}$	3.3, 10, 30	Burst duration factor.
$f_{\rm df}$	0.5, 1.5, 4.5	Rescaling factor for the dynamical friction time-scale.

$\gamma' \approx 0.5$ at $z = 0$ in our reference model. In this halo mass regime above the SHM break, effective AGN feedback means that stellar mass assembly is dominated by galaxy mergers rather than by star formation. Without galaxy mergers, stellar mass assembly would stop entirely, such that passive galaxies would evolve along a power law with exponent $\gamma' = 0$ as their host haloes continue to grow in mass. In the opposite extreme where infalling satellite galaxies instantly merge on to the central galaxy after a halo merger, the expectation is instead that stellar mass assembly will simply trace the hierarchical halo assembly process. In this case, passive central galaxies evolve along a power law with exponent $\gamma' = 1$.

In reality, satellite galaxies merge a finite period of time after infall. The evolution in our model form $\gamma' \approx 0$ at $z = 4$ to $\gamma' \approx 0.5$ at $z = 0$ therefore simply reflects that there is a latency between halo and satellite galaxy mergers, such that γ' is pushed to higher values with cosmic time.

5 DEPENDENCE ON INDIVIDUAL MODEL PARAMETERS

The top panels in Fig. 4 shows that in our reference model, the lack of significant evolution in the predicted median SHM relation is driven primarily by a characteristic evolutionary path that star-forming galaxies follow across the SHM plane. For star-forming galaxies to evolve in this way requires a fairly specific evolution in the instantaneous star formation efficiency, $\eta_{\rm SF}$. This raises the question of whether this characteristic evolutionary path is a general prediction made by semi-analytic galaxy formation models such as GALFORM, or just a feature specific to the combination of model parameters used in our reference model.

To address this question, we now explore the evolution of the SHM relation predicted by models with alternative sets of model parameters. Changing individual model parameters in isolation will typically result in models that give a poor match to the local galaxy luminosity function. None the less, this exercise is still useful for giving us an idea about the effect that each parameter has on the evolution of the median SHM relationship. A list of the model parameters which we consider for this exercise is presented in Table 1.

The results for the range in evolution of the SHM relation predicted by this model suite are shown in Figs 5 and 6. In Fig. 5, we show the evolution in the fitting parameters for the parametric SHM relation given by equation (8). Comparing each variant model in turn with the reference model, it is clear that the modest evolution in the SHM relation predicted by the reference model is not a general prediction of GALFORM. Instead, the reference model appears to occupy a unique position in the overall parameter space (at least for a subset of the model parameters). It should be noted that the parameter variations that we consider here are large. In our experience, these large parameter variations can push the model outside of the regime of efficiencies and time-scales occupied by our reference model (that lead to a non-evolving SHM relation). This is the regime of short gas depletion time-scales in galaxy discs, strong SNe feedback that scales exactly with halo properties, constant gas reincorporation efficiency, and where AGN feedback is very efficient when haloes become hydrostatic.

Fig. 6 shows an alternative view of the range in evolution seen in Fig. 5, this time considering the evolution in fixed halo mass bins. Here, it becomes apparent that our reference model is most distinct from at least some of the variant models presented in Table 1 in the $\log(M_{\rm H}) = 11.6, 12.6$ mass range. We note that these are the bins that approximately bracket the SHM break mass, M_1. For the other two bins at the lowest and highest halo masses considered ($\log(M_{\rm H}) = 10.6, 13.6$), our reference model is more typical of the variant models we consider here for the predicted evolution.

6 ALTERNATIVE MODELS

Figs 5 and 6 show that the small amount of evolution in the SHM relation seen for our reference model is not a general prediction of all GALFORM models. However, the set of models considered in Section 5 did not, in general, produce an acceptable match to the local stellar mass function. This then raises the question of how much variation in the evolution of the SHM relation can be predicted by a family of models that do provide an adequate fit to the local stellar mass function inferred from observations. Another way to phrase this question is to ask the following: to what extent does the form of the local stellar mass function inferred from observations constrain galaxy formation models to predict a specific type of evolution in the SHM relation?

To answer this question properly would require constructing a full posterior distribution from the model parameter space to find all acceptable models, using the local stellar mass function as a constraint. Here, we take an intermediate step by instead considering

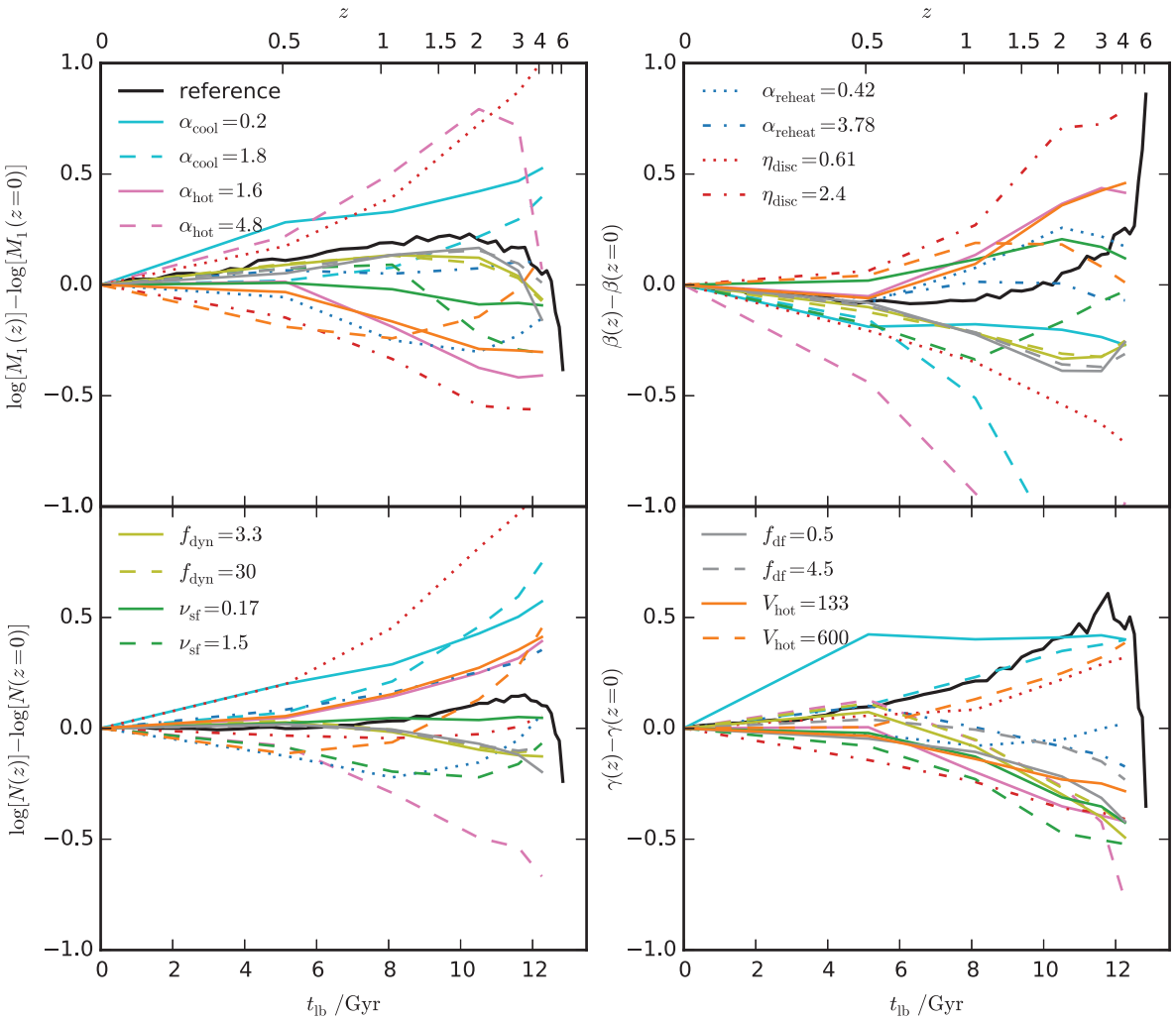

Figure 5. Evolution with respect to $z = 0$ of fitting parameters for the median SHM relation (see equation 8). Each line shows the median of the projected posterior distribution for a given parameter and model, as labelled. Each model has a single parameter varied with respect to the reference model (black line), as described in Table 1. Note that the key is spread over all four panels.

only a limited number of different models which have been tuned to roughly match the local stellar mass function. These models encapsulate some of the variations which, through experience, we expect to be interesting within the context of exploring why our reference model predicts very little evolution in the SHM relation.

Specifically, we consider five additional models, with model parameters outlined in Table 2. Two of these models represent variations of the reference model. They use the same physics parametrizations as the reference model. These two variant models are chosen to highlight that there is a degeneracy between the reincorporation rate coefficient, $\alpha_{\rm reheat}$, and the normalization of the mass loading factor, $V_{\rm hot}$. By either raising or lowering both of these parameters together, it is possible to preserve roughly the same stellar mass function as the reference model. This process also requires a slight adjustment to the AGN feedback threshold parameter, $\alpha_{\rm cool}$ to keep the break of the stellar mass function at the correct stellar mass. We refer to these two variant models as the strong feedback (SFB, high mass loading, fast reincorporation) and the weak feedback (WFB, low mass loading, slow reincorporation) models.

The other three models which we consider here are the three models presented in Mitchell et al. (2014). For this paper, we are primarily interested in the two models from Mitchell et al. (2014) that featured modified parametrizations for the reincorporation time-scale. However, the models presented in Mitchell et al. (2014) were run on merger trees extracted from the original Millennium simulation, which assumed a *WMAP*-1 cosmology (Springel et al. 2005). Therefore, to act as a point of comparison for these two modified reincorporation models, we also include the reference model from Mitchell et al. (2014). In this paper, we refer to the reference model from Mitchell et al. (2014) as the M14 model. In addition to the changes in cosmological parameters, the three models taken from Mitchell et al. (2014) also use the updated cooling scheme from Benson & Bower (2010). For reference, the default GALFORM reincorporation time-scale parametrization (as used in the M14, reference, SFB and WFB models) is given by equation (7) in Section 2.1.

The first of the two modified reincorporation models from Mitchell et al. (2014) which we consider here, referred to as the star formation history (SFH) model, was designed to try to reproduce the star formation histories for star-forming galaxies inferred from observations. For all but the most massive star-forming galaxies, this model reproduces the trend implied by observational data that the specific star formation rate at fixed stellar mass has declined

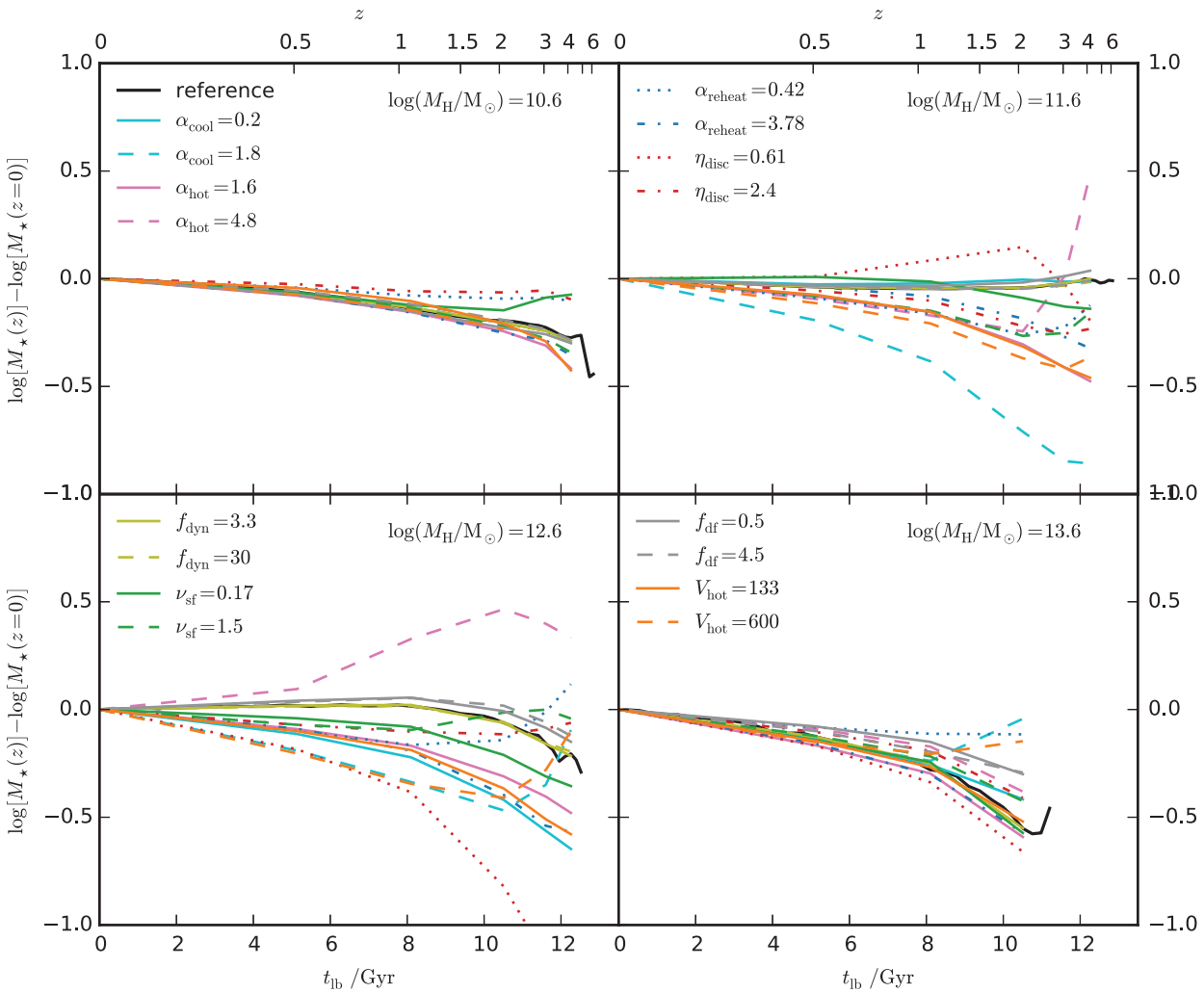

Figure 6. Evolution with respect to $z = 0$ in the median stellar mass within a given halo mass bin. Each panel corresponds to a different halo mass bin, as labelled. Each line shows the evolution in the median stellar mass for a given model, relative to the median stellar mass at $z = 0$. Each model has a single parameter varied with respect to the reference model (black line), as described in Table 1. Note that the key is spread over all four panels.

Table 2. Model parameters used in the five variant models explored in Section 6. $\alpha_{\rm hot}$ sets the mass loading dependence on circular velocity, $V_{\rm hot}$ sets the mass loading normalization, $\alpha_{\rm reheat}$ sets the reincorporation rate and $\alpha_{\rm cool}$ controls the AGN feedback threshold. The variant models considered here include the SFB and WFB, which feature stronger/weaker feedback but with shorter/longer reincorporation time-scales to compensate. M14 is the reference model from Mitchell et al. (2014). The SFH and VM models feature different modifications to the reincorporation time-scale, as described in the text.

Model parameter	Reference	SFB	WFB	M14	SFH	VM
$\alpha_{\rm hot}$	3.2	3.2	3.2	3.2	3.2	3.2
$V_{\rm hot}$ /km s^{-1}	425	700	300	485	485	485
$\alpha_{\rm reheat}$	1.26	8.0	0.3	1.26	0.023	0.24
$\alpha_{\rm cool}$	0.6	0.65	0.4	1.0	1.3	1.0

exponentially from high redshift to today. With respect to our reference model, the SFH model uses a different parametrization for the reincorporation rate, $\dot{M}_{\rm ret}$, given by

$$\dot{M}_{\rm ret} = \frac{\alpha_{\rm reheat}}{t_{\rm dyn}} \left(\frac{M_{\rm H}}{10^{10} h^{-1}\,{\rm M}_\odot} \right) F(z) M_{\rm res}, \quad (22)$$

where $t_{\rm dyn}$ is the halo dynamical time and $F(z)$ is a function of redshift given by

$$\log[F(z)] = 6\,\exp\left[-\frac{(1+z)}{3}\right]\,\log_{10}[1+z]. \quad (23)$$

This parametrization has no physical motivation and essentially just represents an empirical fit to the peaked star formation histories inferred for star-forming galaxies in Mitchell et al. (2014). This is achieved by making reincorporation rates very slow at early times when haloes have yet to accrete most of their mass. The exponential function then dramatically lengthens the reincorporation time-scale at late times to achieve the exponential drop in star formation rates implied by observational data.

The final model from Mitchell et al. (2014), referred to here as the virial mass (VM) model, uses the reincorporation parametrization advocated by Henriques et al. (2013, 2015). This parametrization is given by

$$\dot{M}_{\rm ret} = \alpha_{\rm reheat} \left(\frac{M_{\rm H}}{10^{10} h^{-1}\,{\rm M}_\odot} \right) \frac{M_{\rm res}}{1\,{\rm Gyr}}. \quad (24)$$

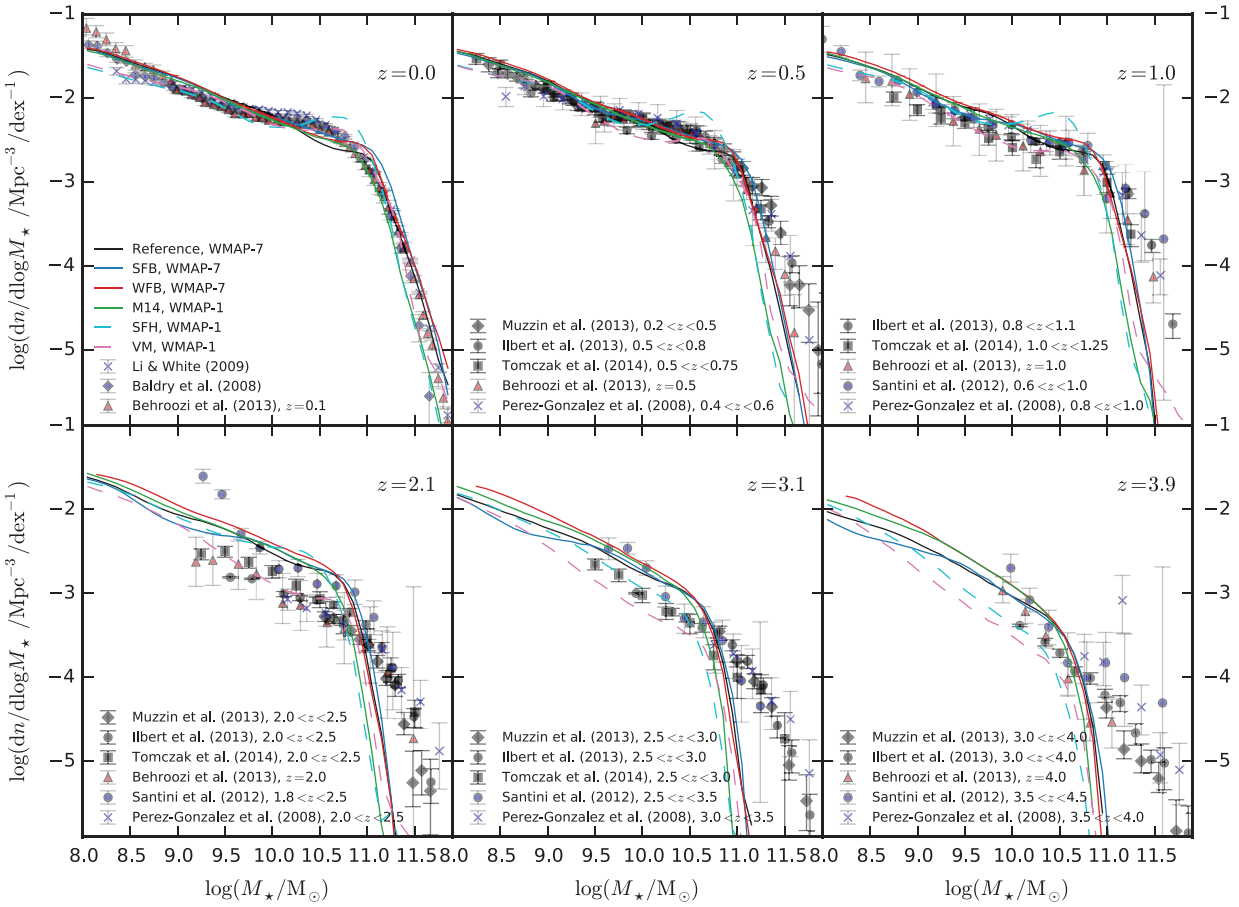

Figure 7. Stellar mass functions for a selection of redshifts for the models described in Table 2. Each line corresponds to a different model, as labelled. Points and associated error bars show observational estimates of the stellar mass function from Baldry et al. (2008), Pérez-González et al. (2008), Li & White (2009), Santini et al. (2012), Behroozi et al. (2013b), Ilbert et al. (2013), Muzzin et al. (2013a) and Tomczak et al. (2014). Points that were used as constraints for abundance matching in Moster13 are shown in blue and those used by Behroozi et al. (2013b) are shown in red.

In appendix C of Mitchell et al. (2014), we showed that this model produces a good fit to the evolution in the stellar mass function below the break inferred from observations.

Before proceeding to analyse the predicted evolution in the SHM relation from the six models presented in Table 2, we first show in Fig. 7 the stellar mass function for a range of redshifts for this family of models. At $z = 0$, none of the models precisely match the shape of the stellar mass function inferred from observations. Specifically, all models underpredict the abundance of galaxies just below the knee. Furthermore, all but the VM and SFH models predict an overabundance of galaxies at the low-mass end (around 10^9–$10^{9.5}\,\mathrm{M}_\odot$). For this analysis however, we simply require that each model give a similar level of agreement as the reference model to the observational estimates of the local stellar mass function. As such, we consider the level of consistency between the models and data shown in the $z = 0$ panel of Fig. 7 to be acceptable for our purposes. We note that in most instances, the level of disagreement between models and data is comparable to the level of disagreement between different observational estimates.

Fig. 8 shows the median SHM relation from the family of models presented in Table 2 for a range of redshifts. Before proceeding to analyse the results, we first note that when comparing the evolution predicted by different models, we expect the most prominent (and interesting) differences between the models will be displayed for halo masses both around and below the break in the SHM relation ($\log(M_\mathrm{H}/\mathrm{M}_\odot) < 12.5$). The reason for this expectation is that this is the halo mass range which contains star-forming galaxies. In more massive haloes, stellar mass assembly takes place primarily through mergers, and the details of the SHM relation will be mainly determined by AGN feedback and the merging parametrizations, which we do not vary outside of adjusting the AGN feedback threshold, α_cool.[12] The variant models here are instead primarily distinct from each other in the parametrizations and parameters adopted for SNe feedback and gas reincorporation. These are processes that mostly affect only the actively star-forming galaxy population.

By examining Fig. 8, it is apparent that for halo masses above the SHM break, all the models display similar (although not identical) evolution in the SHM relation. This presumably reflects the fact that we do not change the AGN feedback model (beyond the threshold) or the galaxy–galaxy merging time-scale between the different models. In detail, the evolution should not be (and is not) identical because, for example, of the role played by low-mass satellites

[12] To first order, α_cool can be considered as a parameter which only controls the break mass in the SHM relation.

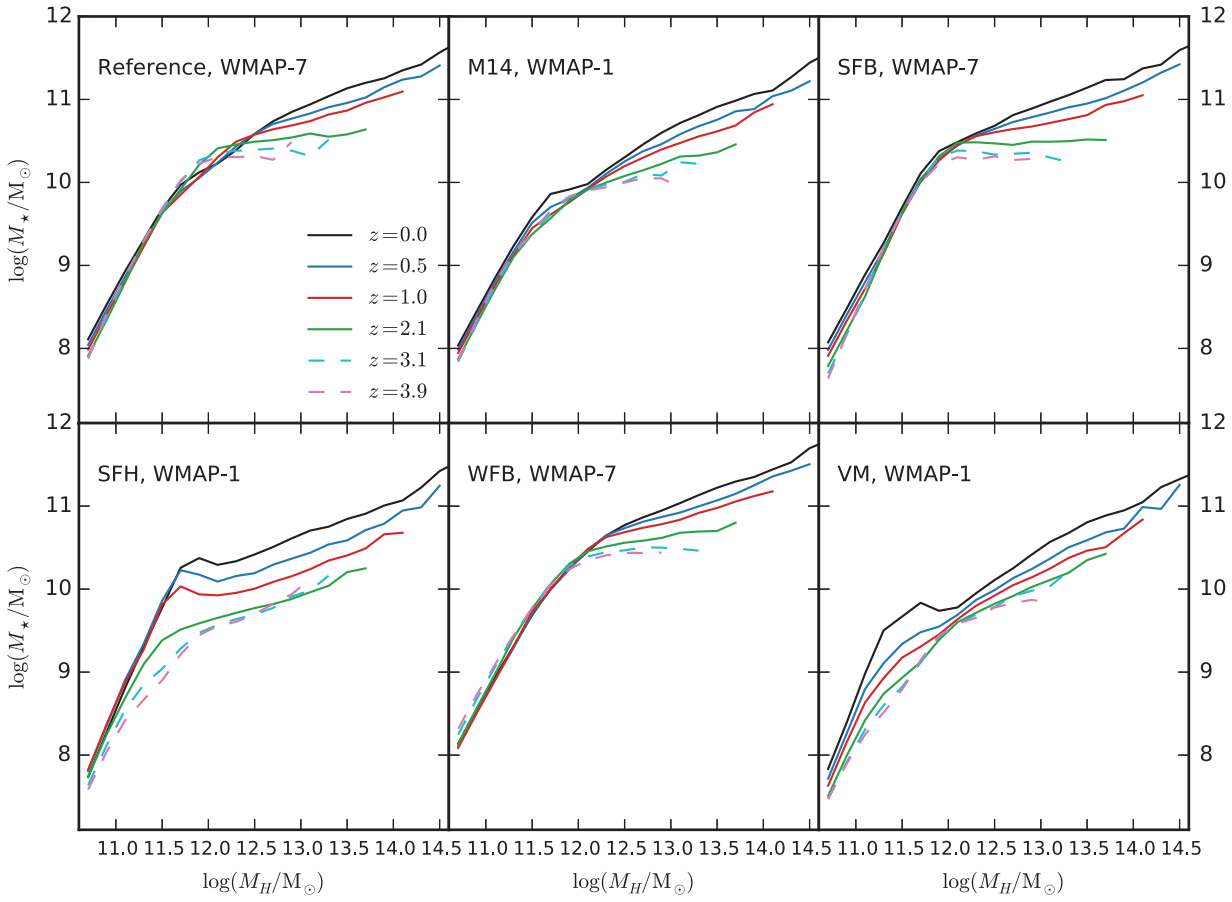

Figure 8. Evolution of the median stellar mass as a function of halo mass for the models described in Table 2. Each panel corresponds to a different model, as labelled, while different lines within a panel show the same model for different redshifts. The cosmological parameter set used for each model is also labelled.

(which are sensitive to the SNe feedback and gas reincorporation physics before infall) in building the stellar mass of massive galaxies through minor mergers.

At and below the break ($\log(M_\mathrm{H}/\mathrm{M}_\odot) < 12.5$), larger variations between some of the models become apparent. Specifically, it can be seen that the trend for the SHM relation below the break to remain approximately constant with redshift is displayed by all the models (reference, WFB, SFB, M14) using the standard reincorporation time-scale. This is not an exact statement and the dynamic range displayed in Fig. 8 is large.[13] Comparatively, the SFH and VM models display much more significant evolution at and below the SHM break. For the SFH model in this halo mass range, the SHM relation evolves significantly for $z \geq 2$ before becoming fixed in place for $z \leq 1$. This can be understood given that the model was designed implicitly to force star formation rates at fixed stellar mass to drop exponentially with cosmic time. The VM model also displays significant evolution in the SHM relation but in this case the evolution also occurs for $z \leq 1$. This behaviour can be understood because the VM model is designed implicitly to increase star formation rates at late times relative to the standard reincorporation parametrization used in the reference, WFB, SFB and M14 models.

[13] The more subtle variations between the reference, WFB, SFB and M14 models are better viewed with lower dynamic range, which we address with subsequent figures.

Another view of the evolution of the SHM relation is shown in Figs 9 and 10, which show the evolution in median stellar mass at fixed halo mass. For these figures, we present the comparison with the SHM evolution inferred using abundance matching from Moster et al. (2013) and Behroozi et al. (2013b). We show the comparison both uncorrected (solid lines) and corrected (dashed lines) for differences with our halo catalogues (see Appendix A). For clarity, as we are now considering a range of models with two different sets of cosmological parameters (*WMAP*-7 and *WMAP*-1), we have split the set of models from Table 2 into two figures. The corrected abundance matching results shown in Fig. 9 are therefore corrected to the GALFORM *WMAP*-7 halo catalogue while the corrected abundance matching results shown in Fig. 10 are corrected to the GALFORM *WMAP*-1 halo catalogue.

Before commenting on the relative evolutionary trends displayed by the different GALFORM models shown in Figs 9 and 10, it is worth underlining that the absolute discrepancies between our models and abundance matching results in median stellar mass at a given halo mass are much larger in some cases than might be expected from comparison of the stellar mass functions shown in Fig. 7. In the lowest halo mass bin shown, the importance of the differences in halo catalogues is clearly underlined as the Moster et al. (2013) median stellar mass shifts down by ≈0.4 dex, into better agreement with our GALFORM models. However, even accounting for differences between halo catalogues, large differences remain. For example, the median stellar mass at $\log(M_\mathrm{H}/\mathrm{M}_\odot) = 12.6$ in the VM model is ≈0.7 dex lower than Moster et al. (2013) and Behroozi et al. (2013b)

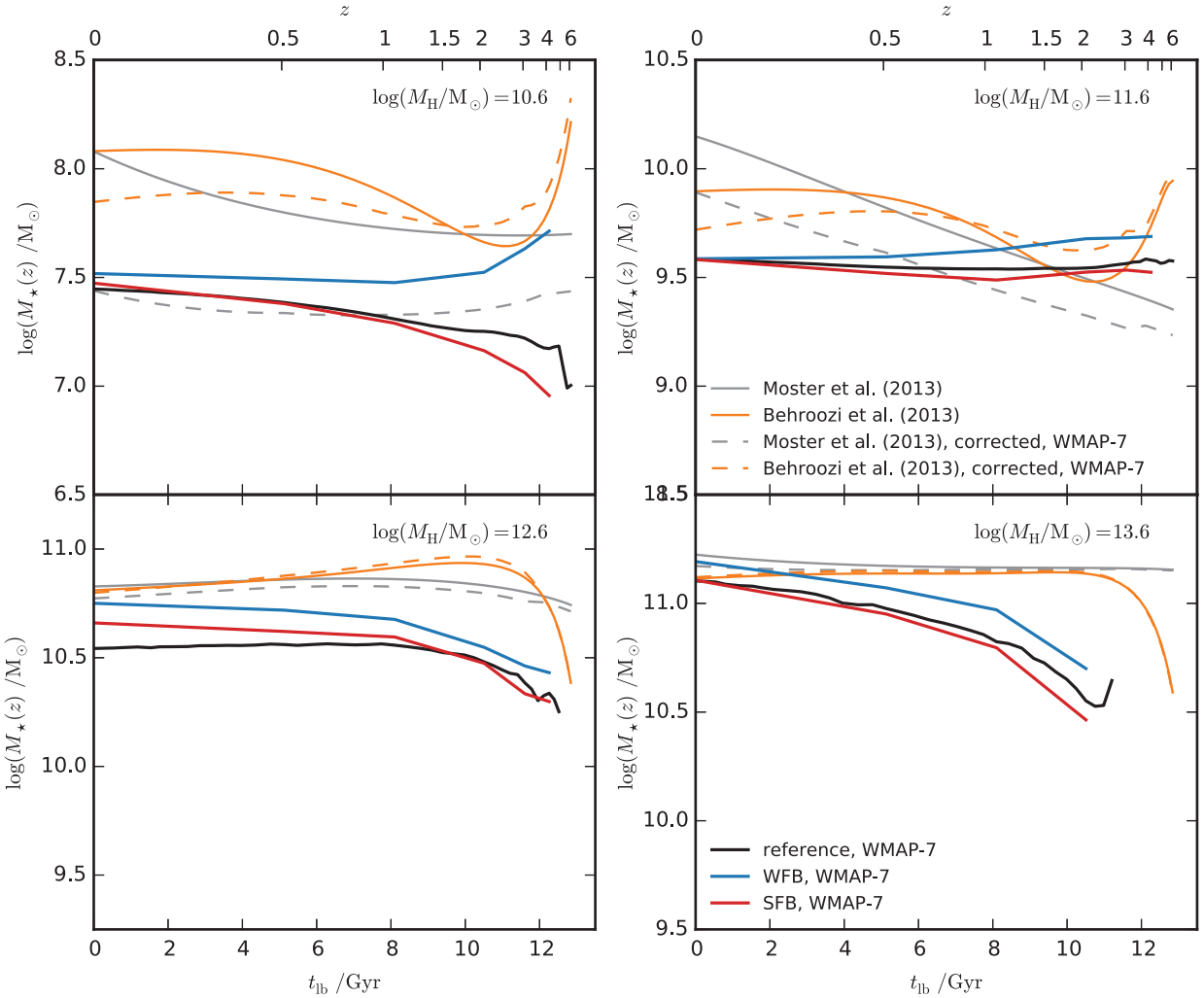

Figure 9. Evolution in the median stellar mass within a given halo mass bin. Each panel corresponds to a different halo mass bin, as labelled. With the exception of grey and orange, solid lines show the median stellar mass for the subset of models described in Table 2 that use a *WMAP*-7 cosmology, as labelled. Grey and brown solid lines show the best-fitting parametric SHM relations from Moster et al. (2013) and Behroozi et al. (2013b), respectively. Moster et al. (2013) and Behroozi et al. (2013b) both assume a *WMAP*-7 cosmology. Grey and brown dashed lines show best-fitting parametric evolution we obtain after correcting the Moster et al. (2013) and Behroozi et al. (2013b) SHM relations to be compatible with the *WMAP*-7 halo catalogues used in GALFORM.

at $z = 0$. Given the fairly good agreement between the stellar mass functions in this model and the observational constraints used by abundance matching at this redshift, and that the effects of halo catalogues have been accounted for, this indicates that there are significant differences in the distribution of stellar mass around the median SHM relation. Indeed, we find that the intrinsic scatter around the median SHM relation is significantly larger in the SFH and VM models ($\sigma \approx 0.5$–0.6 dex) compared to the other models with standard gas reincorporation ($\sigma \approx 0.4$ dex). It should also be noted that constraints inferred from observations imply that the scatter should be significantly smaller, at $\sigma \approx 0.15$–0.2 dex (see Appendix B).

Returning our attention to the relative evolutionary trends shown by different models in Figs 9 and 10, we see that, as in Fig. 8, the VM and SFH models are clearly distinct from the other GALFORM models in that they predict significant evolution in the $\log(M_{\rm H}/{\rm M}_{\odot}) = 11.6$ bin. This is also the bin where the abundance matching results display the most significant evolution. Again, it is apparent that all of the models predict very similar evolutionary trends for the most massive haloes ($\log(M_{\rm H}/{\rm M}_{\odot}) = 13.6$ bin). It is interesting to note that this trend seen in the models is contrary to abundance matching results which imply minimal evolution in this halo mass range. Given that the abundance matching results reproduce (by construction) the evolution of the stellar mass function inferred from observations, and that all of the models we consider here fail to reproduce the abundances of galaxies at the massive end of the stellar mass function at higher redshifts[14] (see Fig. 7), this implies that the models ought to be changed such that the SHM relation does not evolve at $\log(M_{\rm H}/{\rm M}_{\odot}) = 13.6$.

Fig. 9 also shows more subtle differences between the models. For example, in the $\log(M_{\rm H}/{\rm M}_{\odot}) = 10.6$ bin, the WFB and SFB models both clearly start to diverge from the reference model in opposite directions for $z \geq 1$. This demonstrates how the degeneracy

[14] This is not accounting for the Eddington bias effect, where due to steep shape of the Schecter function above the break, random stellar mass errors will preferentially up-scatter galaxies into the exponential tail of the distribution. This can lead to a significant overestimate of the abundance of galaxies above the exponential break in the stellar mass function.

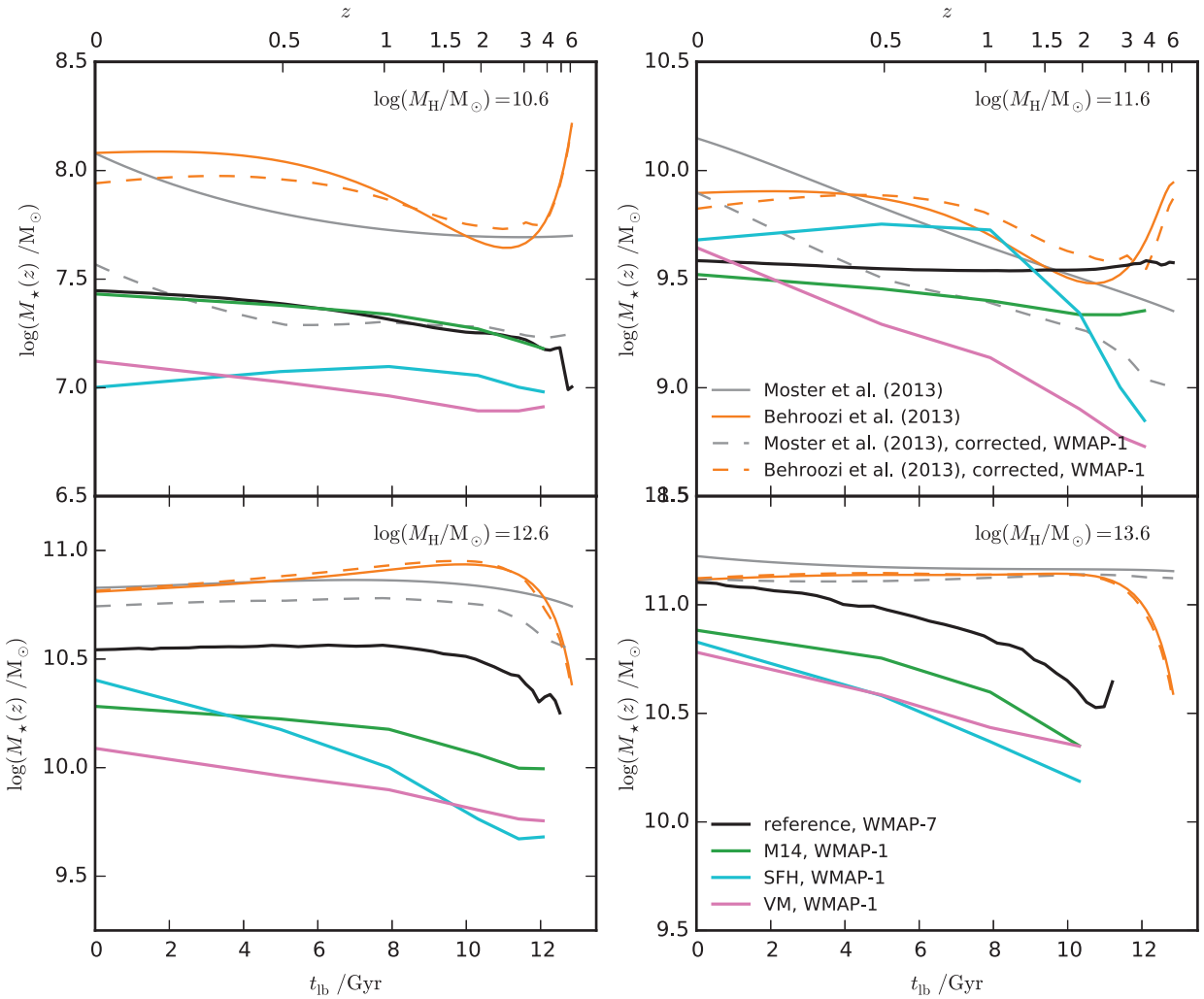

Figure 10. Evolution in the median stellar mass within a given halo mass bin. Each panel corresponds to a different halo mass bin, as labelled. With the exception of grey and brown, solid lines show the median stellar mass for the subset of models described in Table 2 that use a *WMAP*-7 cosmology, as labelled. Grey and orange solid lines show the best-fitting parametric SHM relations from Moster et al. (2013) and Behroozi et al. (2013b), respectively. Moster et al. (2013) and Behroozi et al. (2013b) both assume a *WMAP*-7 cosmology. Grey and brown dashed lines show best-fitting parametric evolution we obtain after correcting the Moster et al. (2013) and Behroozi et al. (2013b) SHM relations to be compatible with the *WMAP*-1 halo catalogues used in GALFORM.

between $\alpha_{\rm reheat}$ and $V_{\rm hot}$ in the SHM relation at $z = 0$ in this halo mass range is broken by considering the evolution.

An alternative view of the evolutionary behaviour in the SHM relation is presented in Fig. 11, which shows the evolution in the fitting parameters from equation (8). In this case, it is only possible to make the comparison with the results from (Moster et al. 2013, as we have adopted their parametrization for the SHM relation). We note that when considering results using the Moster et al. (2013) SHM parametrization given by equation (8), it should be kept in mind that this parametrization does not provide a good fit to the SHM relations in the SFH and VM models at lower redshifts (see Fig. 8).

Starting with the break mass in the SHM relation, M_1, Fig. 11 shows that the models we consider predict very little evolution. The exception is the VM model, which predicts that the break mass drops by $\sim$0.7 dex between $z = 0$ and 4. This is in contrast to the trend inferred from Moster et al. (2013), who favour an increase in the break mass towards high redshift. For the normalization of the SHM relation at the break, N, most of the models we consider predict minimal evolution, consistent with Moster et al. (2013). The exceptions are the VM and SFH models, where N starts to increase after $z = 0.5$ and 1, respectively.

For the low-mass SHM slope, β, the differences between the different models become more apparent. The WFB and SFB models again bracket the evolution predicted by the reference model. The VM and SFH models predict that β increases substantially with lookback time, in contrast to the M14 model and Moster et al. (2013), demonstrating the importance of the reincorporation time-scale parametrization in galaxy formation models. For the high-mass SHM slope, γ, the models we consider all predict fairly modest evolution, consistent with Moster et al. (2013).

7 DISCUSSION

As a diagnostic of galaxy formation models, comparing the median SHM relation predicted by competing models with the results of abundance matching can provide complementary information to a comparison between model predictions and observational estimates of the stellar mass function. If a given galaxy formation model reproduces the observational estimates of the stellar mass function

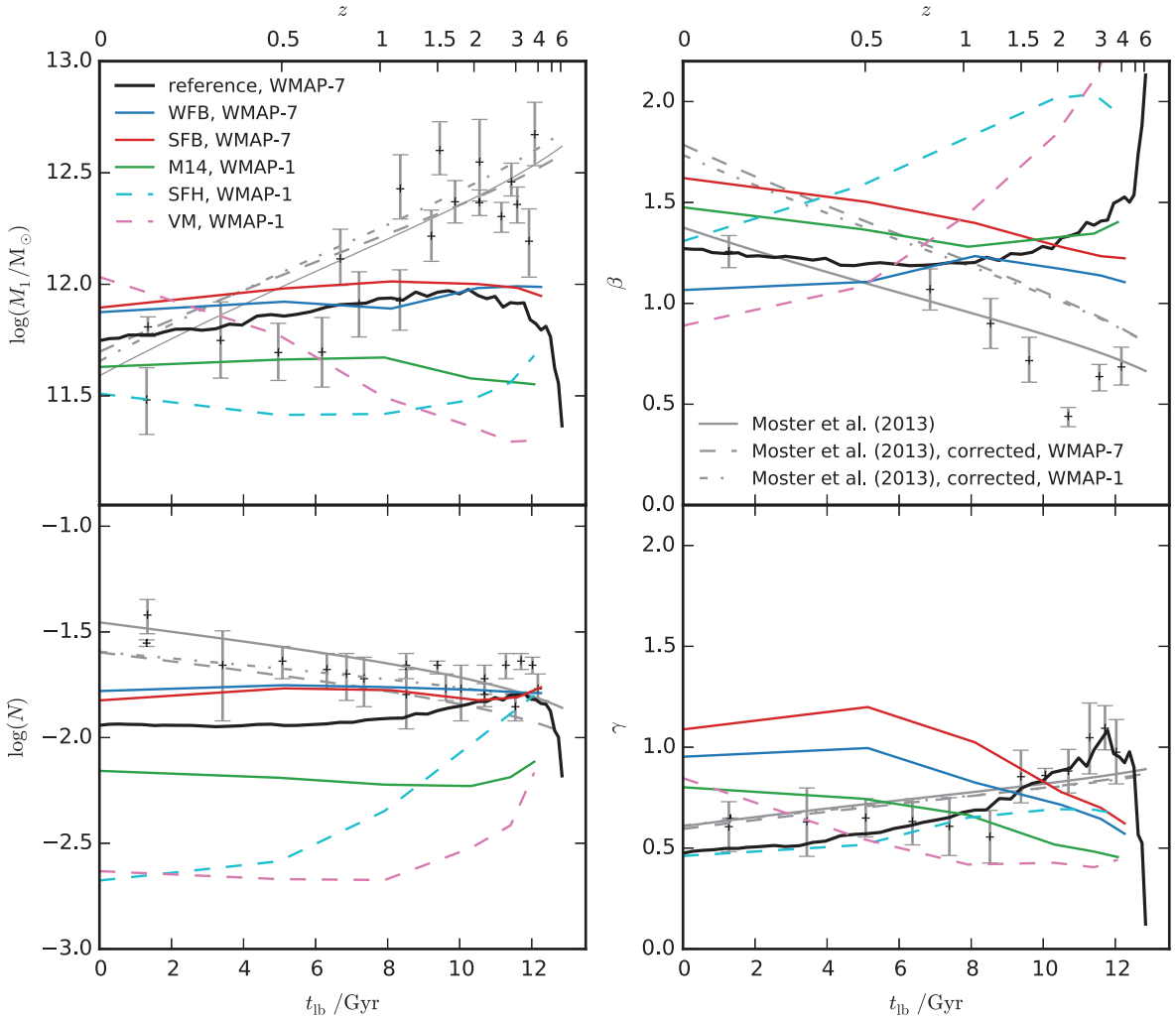

Figure 11. Evolution in fitting parameters for the median SHM relation. Lines (with the exception of grey) show the median of the projected posterior distribution for the models described in Table 2, as labelled. The cosmology used for each model is also labelled. Grey solid lines show the best-fitting parametric evolution determined by Moster et al. (2013) using multi-epoch abundance matching, assuming a *WMAP*-7 cosmology. Grey data points show the associated best-fitting SHM parameters and 1σ error bars determined by Moster et al. (2013) using single epoch abundance matching applied to individual stellar mass functions from the literature. Grey dashed lines show the best-fitting parametric evolution we obtain after correcting the Moster et al. (2013) SHM relation to be compatible with the *WMAP*-7 halo catalogues used in GALFORM. Grey dash–dotted lines show the same information but corrected to be compatible with *WMAP*-1 halo catalogues.

that were used to constrain an abundance matching model, then any differences in the predicted versus inferred median SHM relation can be interpreted as a problem in the galaxy formation model with the distribution in stellar mass around the median SHM relation. The two caveats to this are first that the halo catalogues used as inputs for the two techniques must be the equivalent. Secondly, the abundance matching itself needs to adequately reproduce the true intrinsic scatter around the median SHM relation (and model potential sources of error on observational data correctly). In Section 5, we highlighted several instances where the median SHM relation inferred using abundance matching was discrepant with specific GALFORM models, despite correcting for differences in halo catalogues. Given that some of these models give reasonable levels of agreement with the observational estimates of the stellar mass function used to constrain abundance matching, one interpretation therefore has to be that the distribution in stellar mass around the median in our models is not the same as for real galaxies.

In Mitchell et al. (2014), we found that it was necessary to modify the parametrization of at least one of the physical processes in our model in order to reproduce the star formation rates of star-forming galaxies inferred from observations. As one of the most uncertain aspects of our modelling approach, we chose to modify the reincorporation time-scale to illustrate this point. However, we then found that explaining the evolution of the stellar mass function requires a contradictory modification to the gas reincorporation time-scale compared to explaining the evolution of star formation rates. Specifically, we introduced the SFH model to reproduce the star formation rate evolution inferred from observations and the VM model to reproduce the evolution of the stellar mass function.[15] Given that these modifications to the reincorporation time-scale have a significant impact on the predicted stellar mass functions and star formation rates, one naturally expects differences to also appear in the predicted evolution of the SHM relation. We find that this is indeed the case close to the break in the SHM relation. However, neither of our modified models predict evolution that

[15] These models are introduced in Section 6.

closely resembles results from the abundance matching studies of Moster et al. (2013) and Behroozi et al. (2013b), despite claims from those studies that they reproduce simultaneously both the star formation rates and the stellar mass assembly inferred from observations. This is interesting, particularly given the problems that have been reported by a wide range of contemporary models and simulations in reproducing evolution in star formation rates and/or stellar mass functions inferred from observations (e.g. Lamastra et al. 2013; Cousin et al. 2015a; Furlong et al. 2015; Sparre et al. 2015), but see Henriques et al. (2015).

As we have discussed, this could reflect problems with the intrinsic distribution of stellar mass around the median stellar mass at a given halo mass. We plan to return to this topic as part of future work (see also the discussion in Appendix B). However, there are other aspects of the models and abundance matching that are worthy of consideration. When considering the problem of reproducing star formation rates and stellar mass functions simultaneously, it is important to be aware that the abundance matching approach does not, at present, distinguish between star-forming and passive galaxy populations at a given halo mass (although see Hearin & Watson 2013; Watson et al. 2015). This is likely to be problematic close to the SHM break mass, where the central galaxy population transitions between dominant star-forming and passive galaxy populations. We note that this is precisely the most interesting halo mass range for distinguishing between the different models considered in our analysis.

Another important consideration is whether recent observational estimates of the stellar mass function from deep Ultra-VISTA (Ilbert et al. 2013; Muzzin et al. 2013a) and ZFOURGE (Tomczak et al. 2014) data display significant differences with respect to older observational estimates, particularly above $z = 2$. From Fig. 7, where these recent estimates can be compared with the estimates used as abundance matching constraints, we conclude that the constraints used by Moster et al. (2013) and Behroozi et al. (2013b) are not obviously in significant disagreement with the more recent observational estimates. At higher redshifts, the Santini et al. (2012) estimate (used as a constraint in Moster et al. 2013) is perhaps too steep at lower stellar masses, and the estimate from Behroozi et al. (2013b) for the stellar mass function at $z = 2$ is perhaps a little low around the knee. However, we would not expect the estimates of the median SHM relation from abundance matching (or other techniques) to change significantly once these more recent data sets are included as constraints.

8 SUMMARY

We have explored the evolution of the median stellar mass versus halo mass (SHM) relation predicted by different versions of the semi-analytic galaxy formation model, GALFORM. For our reference model, where the return time-scale for gas ejected from galaxies by SNe feedback scales with the halo dynamical time-scale, we find that the median SHM evolves only very modestly between $z = 0$ and 4. This implies that the efficiency of stellar mass assembly (star formation plus galaxy mergers) within haloes at fixed halo mass is approximately independent of cosmic time (see Behroozi, Wechsler & Conroy 2013a, for a discussion of this point). In our model, this behaviour is primarily driven by the evolution of the efficiency of SNe feedback in regulating star formation rates of actively star-forming galaxies. This SNe efficiency drops as haloes grow in mass, such that star-forming galaxies evolve along a fixed power law in the SHM plane, given by $M_\star \propto M_{\rm H}^{2.3}$. Another factor that causes there to be minimal evolution in the predicted SHM relation is the AGN feedback model implemented within GALFORM. Specifically, we show that the threshold for AGN feedback to become effective at suppressing gas cooling in haloes corresponds to a halo mass which is only weakly dependent on cosmic time. This causes the break mass in the SHM relation predicted by GALFORM to evolve only very modestly.

To reproduce the shape of the local stellar mass function inferred from observations places strong constraints on the form of the median SHM relation at $z = 0$. We show that with this single constraint in place, standard[16] semi-analytic galaxy formation models tend not to predict significant evolution in the SHM relation. This behaviour is broken close to the SHM break mass (which is closely connected to the knee of the stellar mass function) for the models introduced in Mitchell et al. (2014) that feature modified gas reincorporation time-scales. At present, abundance matching studies (Behroozi et al. 2013b; Moster et al. 2013) do not strongly support either of these modified GALFORM models. Our preliminary interpretation of this disagreement is that there could likely be a problem in our modified models with, at a given halo mass, the form of the distribution in stellar mass around the median SHM relation. We conclude therefore that there is a clear opportunity to use constraints from the full distribution in stellar mass as a function of halo mass, inferred using empirical modelling of observational data, to improve theoretical galaxy formation models.

ACKNOWLEDGEMENTS

We thank Qi Guo for making catalogues from the L-galaxies semi-analytic galaxy formation model available to us. We thank Idit Zehavi for reading and providing comments that helped improve the clarity of this paper. This work was supported by the Science and Technology Facilities Council [ST/J501013/1, ST/L00075X/1]. This work used the DiRAC Data Centric system at Durham University, operated by the Institute for Computational Cosmology on behalf of the STFC DiRAC HPC Facility (www.dirac.ac.uk). This equipment was funded by BIS National E-infrastructure capital grant ST/K00042X/1, STFC capital grant ST/H008519/1, and STFC DiRAC Operations grant ST/K003267/1 and Durham University. DiRAC is part of the National E-Infrastructure.

REFERENCES

Baldry I. K., Glazebrook K., Driver S. P., 2008, MNRAS, 388, 945
Baugh C. M., 2006, Rep. Prog. Phys., 69, 3101
Behroozi P. S., Conroy C., Wechsler R. H., 2010, ApJ, 717, 379
Behroozi P. S., Wechsler R. H., Conroy C., 2013a, ApJ, 762, L31
Behroozi P. S., Wechsler R. H., Conroy C., 2013b, ApJ, 770, 57
Benson A. J., 2010, Phys. Rep., 495, 33
Benson A. J., 2014, MNRAS, 444, 2599
Benson A. J., Bower R., 2010, MNRAS, 405, 1573
Berlind A. A., Weinberg D. H., 2002, ApJ, 575, 587
Blitz L., Rosolowsky E., 2006, ApJ, 650, 933
Bower R. G., Benson A. J., Malbon R., Helly J. C., Frenk C. S., Baugh C. M., Cole S., Lacey C. G., 2006, MNRAS, 370, 645
Bryan G. L., Norman M. L., 1998, ApJ, 495, 80
Cole S., Lacey C. G., Baugh C. M., Frenk C. S., 2000, MNRAS, 319, 168
Conroy C., Wechsler R. H., Kravtsov A. V., 2006, ApJ, 647, 201
Contreras S., Baugh C. M., Norberg P., Padilla N., 2015, MNRAS, 452, 1861

[16] By this, we mean models where the efficiency of gas reincorporation after ejection by feedback evolves only weakly with cosmic time.

Cousin M., Lagache G., Bethermin M., Blaizot J., Guiderdoni B., 2015a, A&A, 575, A32
Cousin M., Lagache G., Bethermin M., Guiderdoni B., 2015b, A&A, 575, A33
Durkalec A. et al., 2015, A&A, 576, L7
Fakhouri O., Ma C.-P., Boylan-Kolchin M., 2010, MNRAS, 406, 2267
Font A. S. et al., 2008, MNRAS, 389, 1619
Furlong M. et al., 2015, MNRAS, 450, 4486
Gonzalez-Perez V., Lacey C. G., Baugh C. M., Lagos C. D. P., Helly J., Campbell D. J. R., Mitchell P. D., 2014, MNRAS, 439, 264
Guo Q., White S., Li C., Boylan-Kolchin M., 2010, MNRAS, 404, 1111
Guo Q. et al., 2011, MNRAS, 413, 101
Guo Q., White S., Angulo R. E., Henriques B., Lemson G., Boylan-Kolchin M., Thomas P., Short C., 2013, MNRAS, 428, 1351
Hearin A. P., Watson D. F., 2013, MNRAS, 435, 1313
Henriques B. M. B., White S. D. M., Thomas P. A., Angulo R. E., Guo Q., Lemson G., Springel V., 2013, MNRAS, 431, 3373
Henriques B. M. B., White S. D. M., Thomas P. A., Angulo R., Guo Q., Lemson G., Springel V., Overzier R., 2015, MNRAS, 451, 2663
Hirschmann M., De Lucia G., Wilman D., Weinmann S., Iovino A., Cucciati O., Zibetti S., Villalobos Á., 2014, MNRAS, 444, 2938
Hudson M. J. et al., 2015, MNRAS, 447, 298
Ilbert O. et al., 2013, A&A, 556, A55
Jiang L., Helly J. C., Cole S., Frenk C. S., 2014, MNRAS, 440, 2115
Komatsu E. et al., 2011, ApJS, 192, 18
Lacey C. G. et al., 2015, preprint (arXiv:e-prints)
Lagos C. D. P., Lacey C. G., Baugh C. M., Bower R. G., Benson A. J., 2011, MNRAS, 416, 1566
Lamastra A., Menci N., Fiore F., Santini P., 2013, A&A, 552, A44
Leauthaud A. et al., 2012, ApJ, 744, 159
Li C., White S. D. M., 2009, MNRAS, 398, 2177
Lu Z., Mo H. J., Lu Y., Katz N., Weinberg M. D., van den Bosch F. C., Yang X., 2014a, MNRAS, 439, 1294
Lu Y., Mo H. J., Lu Z., Katz N., Weinberg M. D., 2014b, MNRAS, 443, 1252
McCracken H. J. et al., 2015, MNRAS, 449, 901
McGee S. L., Bower R. G., Balogh M. L., 2014, MNRAS, 442, L105
Mandelbaum R., Seljak U., Kauffmann G., Hirata C. M., Brinkmann J., 2006, MNRAS, 368, 715
Marchesini D., van Dokkum P. G., Förster Schreiber N. M., Franx M., Labbé I., Wuyts S., 2009, ApJ, 701, 1765
Mitchell P. D., Lacey C. G., Baugh C. M., Cole S., 2013, MNRAS, 435, 87
Mitchell P. D., Lacey C. G., Cole S., Baugh C. M., 2014, MNRAS, 444, 2637
More S., van den Bosch F. C., Cacciato M., Mo H. J., Yang X., Li R., 2009, MNRAS, 392, 801
Moster B. P., Somerville R. S., Maulbetsch C., van den Bosch F. C., Macciò A. V., Naab T., Oser L., 2010, ApJ, 710, 903
Moster B. P., Naab T., White S. D. M., 2013, MNRAS, 428, 3121
Muzzin A. et al., 2013a, ApJS, 206, 8
Muzzin A. et al., 2013b, ApJ, 777, 18
Navarro J. F., Frenk C. S., White S. D. M., 1997, ApJ, 490, 493
Peacock J. A., Smith R. E., 2000, MNRAS, 318, 1144
Peng Y.-j. et al., 2010, ApJ, 721, 193
Pérez-González P. G. et al., 2008, ApJ, 675, 234
Reddick R. M., Wechsler R. H., Tinker J. L., Behroozi P. S., 2013, ApJ, 771, 30
Rodríguez-Puebla A., Avila-Reese V., Drory N., 2013, ApJ, 767, 92
Santini P. et al., 2012, A&A, 538, A33
Schaye J. et al., 2015, MNRAS, 446, 521
Scoccimarro R., Sheth R. K., Hui L., Jain B., 2001, ApJ, 546, 20
Shankar F. et al., 2014, ApJ, 797, L27
Somerville R. S., Davé R., 2015, ARA&A, 53, 51
Somerville R. S., Hopkins P. F., Cox T. J., Robertson B. E., Hernquist L., 2008, MNRAS, 391, 481
Sparre M. et al., 2015, MNRAS, 447, 3548
Springel V., White S. D. M., Tormen G., Kauffmann G., 2001, MNRAS, 328, 726
Springel V. et al., 2005, Nature, 435, 629
Tinker J., Kravtsov A. V., Klypin A., Abazajian K., Warren M., Yepes G., Gottlöber S., Holz D. E., 2008, ApJ, 688, 709
Tomczak A. R. et al., 2014, ApJ, 783, 85
Vale A., Ostriker J. P., 2004, MNRAS, 353, 189
Velander M. et al., 2014, MNRAS, 437, 2111
Vogelsberger M. et al., 2014, MNRAS, 444, 1518
Wake D. A. et al., 2011, ApJ, 728, 46
Wang L. et al., 2013, MNRAS, 431, 648
Watson D. F., Conroy C., 2013, ApJ, 772, 139
Watson D. F. et al., 2015, MNRAS, 446, 651
Wetzel A. R., Tinker J. L., Conroy C., 2012, MNRAS, 424, 232
Wetzel A. R., Tinker J. L., Conroy C., van den Bosch F. C., 2013, MNRAS, 432, 336
White C. E., Somerville R. S., Ferguson H. C., 2015, ApJ, 799, 201
Yang X., Mo H. J., van den Bosch F. C., 2003, MNRAS, 339, 1057
Yang X., Mo H. J., van den Bosch F. C., 2009, ApJ, 695, 900
Yang X., Mo H. J., van den Bosch F. C., Zhang Y., Han J., 2012, ApJ, 752, 41
Zehavi I., Patiri S., Zheng Z., 2012, ApJ, 746, 145
Zu Y., Mandelbaum R., 2015, MNRAS, 454, 1161

APPENDIX A: HALO MASSES AND SATELLITE ABUNDANCES

Here, we describe how we attempt to account for differences in the definition of halo mass and in the abundance of satellites between the GALFORM model and the abundance matching studies of Moster et al. (2013) and Behroozi et al. (2013b). In brief, we match the input halo catalogues used by these two studies to correct their reported SHM relations to be consistent with the halo catalogues used in GALFORM.

To do this, we require realizations of the halo catalogues used as inputs by Moster et al. (2013) and Behroozi et al. (2013b). For the case of Moster et al. (2013), we also need to know the distribution of infall redshifts for satellite galaxies. For this purpose, we have made use of an L-galaxies model which was run using the same MR7 simulation that was used in our reference model (Guo, private communication). Compared to GALFORM, the L-galaxies model uses the same SUBFIND subhalo catalogues as inputs but uses halo mass definitions and assumptions about satellites which are the same as those adopted by Moster et al. (2013). Specifically, L-galaxies uses a mean halo density of 200 times the critical density (M_{200}) to define halo mass, and a dynamical friction time-scale is used to decide how long satellite galaxies survive after their subhalo can no longer be identified in the simulation (Guo et al. 2011; Moster et al. 2013).

For the case of Behroozi et al. (2013b), we simply generate a Monte Carlo realization of their halo catalogue using the corrected Tinker et al. (2008) halo mass function and the satellite fractions reported in appendix C of Behroozi et al. (2013b). Behroozi et al. (2013b) define halo masses using the virial overdensity criterion predicted by the spherical collapse model (Bryan & Norman 1998). We note that unlike Moster et al. (2013), Behroozi et al. (2013b) do not include a population of orphan satellites (satellite galaxies with no identifiable subhalo in the simulation), which we will refer to as Type 2 satellites. We refer to satellites for which the subhalo can still be identified in the simulation as Type 1 satellites.

The importance of accounting for the different halo catalogues used by our model, Moster et al. (2013) and Behroozi et al. (2013b) is illustrated in Fig. A1. We show the halo mass functions, satellite-to-central ratios and the resulting stellar mass functions from the three models at $z = 0$. The central halo mass functions from GALFORM

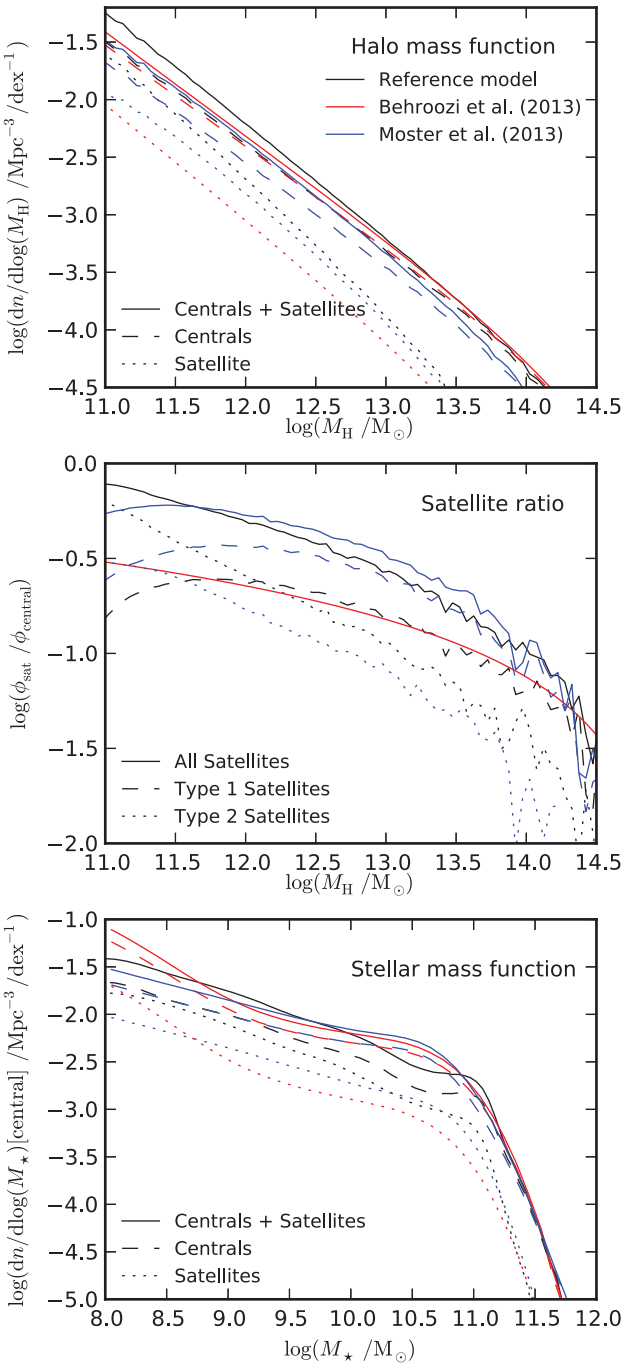

Figure A1. Mass functions at $z = 0$ from our reference GALFORM model (black) and from (Moster et al. 2013, blue) and (Behroozi et al. 2013b, red). Top: halo mass functions, using the halo mass definitions used by each study to quantify the SHM relationship. Solid lines show combined central plus satellite halo mass functions, using the subhalo mass at infall for satellites. Dashed lines and dotted lines show the halo mass functions for central and satellite galaxies respectively. Middle: ratio of the satellite halo to the central halo mass functions, as a function of halo mass. Solid lines show the ratio for all satellites. Dashed lines and dotted lines show the ratio for Type 1 and Type 2 satellites, respectively. Bottom: stellar mass functions for all galaxies (solid lines), central galaxies (dashed lines) and satellite galaxies (dotted lines, includes both Type 1 and Type 2 satellites).

and Behroozi et al. (2013b) are almost indistinguishable (they use similar halo mass definitions) while the Moster et al. (2013) central halo mass function is systematically offset to lower halo mass at a given number density. The offset in $\log(M_{\rm H}/{\rm M}_\odot)$ is $\approx$0.16 dex.

For satellite galaxies, there is a reasonable agreement in the ratio of satellites (Type 1 plus Type 2) to centrals between GALFORM and Moster et al. (2013). There is however a difference in the relative fractions of Type 1 compared to Type 2 satellites between the two halo catalogues. This primarily reflects the fact that in GALFORM, all satellites are allocated an analytically calculated dynamical friction merging time-scale at infall, instead of when the subhalo is lost from the simulation, as is the case in Moster et al. (2013). For the Behroozi et al. (2013b) halo catalogue, the satellite to central ratio is significantly smaller than in the GALFORM or Moster et al. (2013) halo catalogues. This presumably reflects in part the decision made by Behroozi et al. (2013b) not to include Type 2 satellites.

The net result of the difference in satellite abundances is reflected in the combined central plus satellite halo mass function (solid lines in the top panel of Fig. A1). We emphasize that it is the combined halo mass function that is relevant for abundance matching. The Moster et al. (2013) combined halo mass function is similar to the GALFORM halo mass function, but with a roughly constant offset in halo mass at fixed number density. The Behroozi et al. (2013b) combined halo mass function agrees with the GALFORM combined mass function for massive haloes (where centrals dominate) but is shallower. This is caused by the smaller abundance of satellites in the Behroozi et al. (2013b) catalogue. We also show the resulting stellar mass functions in the bottom panel of Fig. A1. For Moster et al. (2013) and Behroozi et al. (2013b), these are produced using their halo catalogues populated using their SHM relations, including intrinsic scatter.

To account for the differences between halo catalogues, we attempt to find a way to correct the Moster et al. (2013) and Behroozi et al. (2013b) SHM relations such that they resemble the SHM relations that they would have obtained if they had performed abundance matching using the GALFORM halo catalogue. Specifically, we search for appropriate mapping functions, $F(M_{\rm H}, z)$, that correct halo masses from the Moster et al. (2013) and Behroozi et al. (2013b) halo catalogues (such that $M_{\rm H,\,corrected} = F(M_{\rm H})M_{\rm H}$). Corrected SHM relations are then obtained by applying their SHM relations to the corrected halo catalogues. The redshift dependence of $F(M_{\rm H}, z)$ reflects that different mapping functions, $F(M_{\rm H})$, will be required to correct the SHM relation for different redshifts. In the case of Moster et al. (2013), we note that for satellites we use a correction factor, $F(M_{\rm H}, z_{\rm infall})$, that corresponds to the infall redshift of the satellite, $z_{\rm infall}$.

To find $F(M_{\rm H}, z)$, we proceed as follows. As a starting point, if we were to consider, for example, the halo catalogue from Behroozi et al. (2013b) at a given redshift, we can apply their SHM relation to both the GALFORM halo catalogue and their catalogue to obtain two cumulative stellar mass functions. If the two halo catalogues differ, then the resulting stellar mass functions will also differ. Our task is to find $F(M_{\rm H}, z)$ such that by applying $F(M_{\rm H}, z)$ as a correction to the halo masses in the Behroozi et al. catalogue before applying their SHM relation to compute a stellar mass function, the resulting cumulative stellar mass functions from the GALFORM and Behroozi et al. halo catalogues are equal.[17] We use this as our constraint

[17] Note therefore that this target stellar mass function is not the stellar mass function predicted by our GALFORM model or the stellar mass function from the empirical Behroozi et al. (2013b) model.

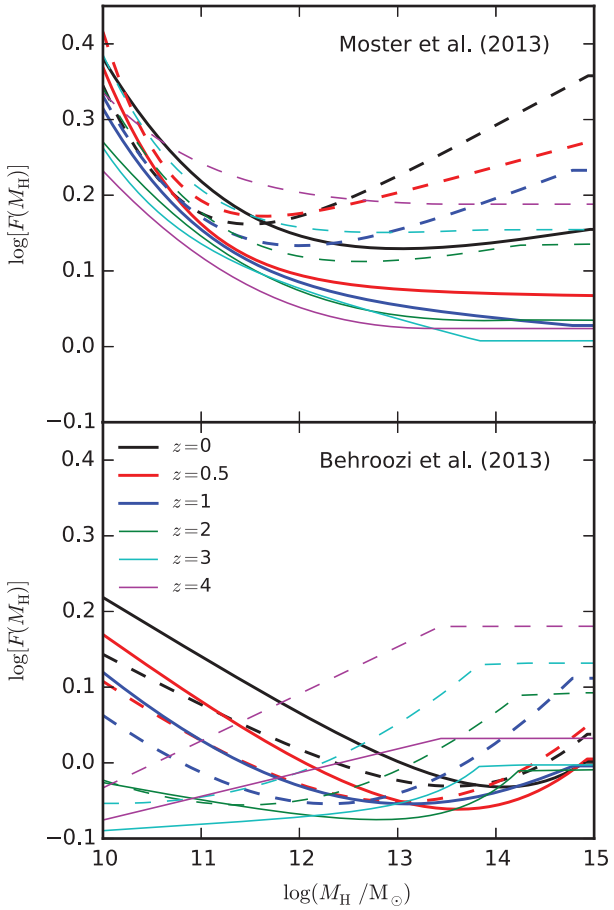

Figure A2. Function $F(M_{\rm H})$ that maps between the halo masses from two different halo catalogues such that, for a given SHM relation, the two catalogues give the same total abundance of galaxies as a function of stellar mass. The top panel shows $F(M_{\rm H})$ computed between the halo catalogues used in GALFORM and a catalogue that is effectively identical to the one used by Moster et al. (2013). Solid lines show $F(M_{\rm H})$ for the GALFORM catalogue taken from the MR7 simulation. Dashed lines show $F(M_{\rm H})$ for the GALFORM catalogue taken from the MILLENNIUM simulation. Different coloured lines correspond to different redshifts, as labelled. The bottom panel shows the corresponding $F(M_{\rm H})$ computed between the halo catalogues used in GALFORM and a Monte Carlo realization of the catalogue used by Behroozi et al. (2013b).

because Moster et al. (2013) and Behroozi et al. (2013b) match abundances as a function of stellar mass.[18]

At a given redshift, we find that a double power law for $F(M_{\rm H})$ is appropriate, with a form given by

$$F(M_{\rm H}) = N_{\rm r}\left[\left(\frac{M_{\rm H}}{M_{\rm r}}\right)^{\alpha_{\rm r}} + \left(\frac{M_{\rm H}}{M_{\rm r}}\right)^{\beta_{\rm r}}\right], \qquad \text{(A1)}$$

where $N_{\rm r}$, $M_{\rm r}$, $\alpha_{\rm r}$ and $\beta_{\rm r}$ are fitting parameters. Once we obtain $F(M_{\rm H})$ for a set of redshifts, we estimate $F(M_{\rm H}, z)$ simply by interpolating $\log[F(M_{\rm H})]$ in $\log(1+z)$. We note that we choose not to extrapolate $F(M_{\rm H})$ for halo masses larger than we can constrain using our halo catalogues at a given redshift. Instead we hold constant $F(M_{\rm H})$ above this mass.

[18] We neglect the fact that Behroozi et al. (2013b) also use other observational constraints to constrain their model parameters.

To estimate values for the fitting parameters in equation (A1), we can obtain a first guess simply by directly matching abundances between two halo catalogues (one from GALFORM and one from either of Moster et al. or Behroozi et al.) as a function of halo mass (instead of stellar mass). For the case of Behroozi et al. (2013b), this first step is all that it is required because in their empirical model, the stellar masses of galaxies depend only on their SHM relation evaluated at the redshift of interest. For the case of Moster et al. (2013), there is an additional complication because they assign satellite galaxies with a stellar mass drawn from the SHM distribution that corresponds to the infall redshift of each satellite, rather than from the distribution corresponding to the desired redshift. Therefore, the abundance of galaxies as a function of stellar mass depends on more than just the halo catalogue at the output redshift. In this case, we have to employ a minimization procedure to refine our initial guess for the fitting parameters in equation (A1).

For the results presented in the main body of this paper, we have computed the mapping functions appropriate for converting SHM relations to be compatible with either our MR7 (*WMAP*-7 cosmology) or MILLENNIUM (*WMAP*-1 cosmology) simulations. We show $F(M_{\rm H}, z)$ as a function of halo mass for the different simulations and abundance matching studies in Fig. A2.

APPENDIX B: INTRINSIC SCATTER IN THE LOCAL SHM DISTRIBUTION

Here, we present the distributions in stellar mass for a set of narrow ($\Delta\log(M_{\rm H}/{\rm M}_{\odot}) = 0.1$ dex) bins in halo mass from our reference model. These are shown in Fig. B1. Our aim is to illustrate that our reference model does not predict that the SHM distribution at fixed halo mass is strictly lognormal, with constant width as a function of halo mass, as is often assumed. To demonstrate this, we fit lognormal distributions both individually to each bin (green lines) and to all bins simultaneously (magenta lines). For low ($M_{\rm H} < 10^{11.5}\,{\rm M}_{\odot}$) and high ($M_{\rm H} > 10^{13.0}\,{\rm M}_{\odot}$) mass haloes, a lognormal distribution appears to provide a good description of the SHM distribution. However, in the intermediate halo mass range, the SHM distribution at fixed halo mass is skewed with respect to a lognormal. Furthermore, from the lognormal distributions that are fit individually to each bin, it is apparent that the intrinsic scatter in the SHM distribution is a function of halo mass, with the scatter peaking at a halo mass of $M_{\rm H} \approx 10^{12.2}\,{\rm M}_{\odot}$.

In the $10^{12.2}\,{\rm M}_{\odot}$ halo mass bin, the distribution is visibly bimodal. We find that this bimodality is best explained by splitting the galaxy population according to how galaxy spheroids assembled their stellar mass. We first consider galaxies where the majority of the stellar mass in the galaxy spheroid was formed as part of quiescent star formation in discs which were subsequently added to the spheroid through either galaxy mergers or disc instabilities. The second population we consider is instead comprised of galaxies where the majority of the stellar mass in the galaxy spheroid was formed in bursts of star formation that took place within galaxy spheroids. In our model, these bursts are triggered by gas accretion on to a spheroid during galaxy merger or disc instability events. Fig. B1 shows that in intermediate mass haloes ($\approx 10^{12.6}\,{\rm M}_{\odot}$), the galaxies with spheroids where the stellar mass was originally assembled by quiescent disc star formation (blue lines) have total stellar masses that are systematically lower than galaxies where the spheroids were assembled in bursts.

To explain this bimodality, we remind the reader that in GALFORM, the mass loading factor for SNe feedback is parametrized as a function of disc circular velocity for star formation in galaxy discs, and

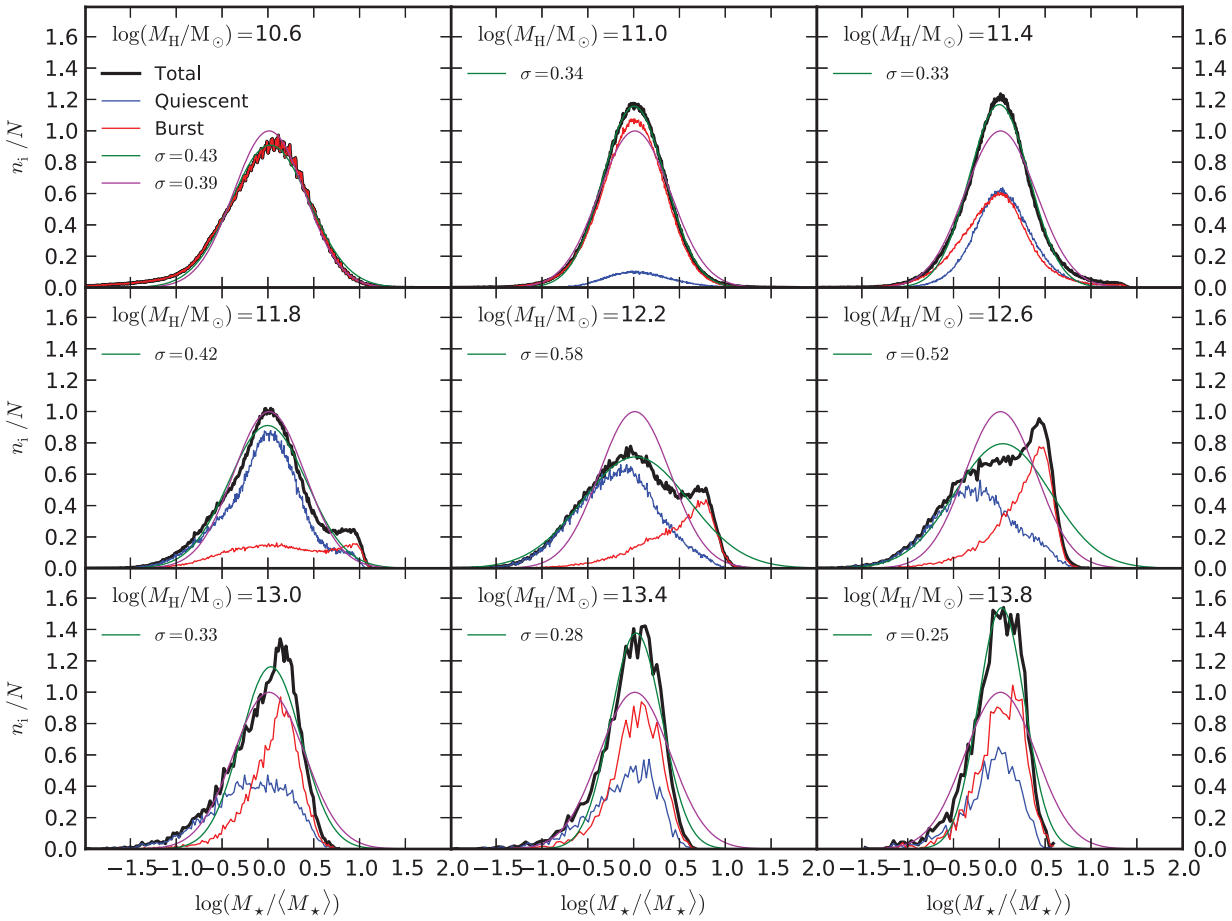

Figure B1. Distributions of stellar mass for the total galaxy population, split into narrow ($\Delta\log(M_{\rm H}/{\rm M}_{\odot}) = 0.1$ dex) bins in halo mass from our reference model at $z = 0$ (black lines). Each panel corresponds to a different halo mass bin, as labelled. For each halo mass bin, we divide stellar masses through by the median stellar mass of the bin. We then fit lognormal distributions individually to each bin (green lines) and to all bins simultaneously (magenta lines). We also show distributions separated on the basis of whether the stellar mass within a given galaxy spheroid was assembled primarily through bursts of star formation (red lines) or through quiescent star formation in galaxy discs which was subsequently added to the spheroid through mergers or disc instabilities (blue lines).

as a function of spheroid circular velocity for star formation taking place in nuclear bursts. In the halo mass range where SNe feedback is strong ($M_{\rm H} < 10^{13}\,{\rm M}_{\odot}$), any systematic differences between typical disc and spheroid circular velocities leads to significantly different mass loading factors for SNe feedback between quiescent and burst star formation channels (which are amplified because of the exponent in the mass loading parametrization, $\alpha_{\rm hot} = 3.2$). This means that at a given halo mass, the efficiency of star formation will depend sensitively on whether star formation takes place in bursts or quiescently in discs. Therefore, in the halo mass range where SNe feedback is strong and the spheroid mass can be significant fraction of the total stellar mass of a given galaxy ($10^{11.8} < M_{\rm H}\,{\rm M}_{\odot} < 10^{13}$), there can be significant differences between $M_{\star}/M_{\rm H}$ at a given halo mass depending on whether bursts or quiescent star formation were the dominant star formation channel for a given galaxy.

We note that the intrinsic scatter predicted by our model systematically exceeds estimates of the scatter obtained using a variety of different empirical techniques that connect observed galaxies with the predicted halo population. Some examples of constraints on the scatter that have been reported include work using group catalogues (0.17 dex; Yang, Mo & van den Bosch 2009), satellite kinematics (0.16 dex; More et al. 2009), a combination of clustering, abundances and lensing (≈0.2 dex; Leauthaud et al. 2012), clustering and group catalogues (0.2, 0.17 dex; Reddick et al. 2013; Rodríguez-Puebla, Avila-Reese & Drory 2013), and a combination of lensing and clustering (0.2 dex; Zu & Mandelbaum 2015). To take a specific example, Reddick et al. (2013) combine subhalo abundance matching with clustering and conditional stellar mass function (estimated using a galaxy group catalogue) constraints to infer the scatter of the SHM relation in the local Universe. They rule out a scatter as large as is predicted by our reference model and find that the intrinsic scatter is not a strong function of stellar mass, which is also in tension with our reference model.

Regarding the tension associated with the amount of mass dependence in the scatter, this could indicate that, either we have overestimated the role of nuclear starbursts in the global stellar mass assembly process, or that the efficiency of SNe feedback should be constant at a given halo mass, irrespective of whether star formation is taking place within discs or spheroids. We note that the latter possibility is assumed in the L-galaxies model (Guo et al. 2011; Henriques et al. 2013), and that the SHM relation in that model does not predict a bimodal feature in the SHM relation at $M_{\rm H} = 10^{12.2}\,{\rm M}_{\odot}$ as a consequence (see fig. 5 in Contreras et al. 2015). This result can be reproduced in GALFORM by simply changing the SNe feedback mass loading parametrization to depend on halo circular velocity. We note that even with this halo circular velocity

dependent SNe feedback efficiency, the resulting SHM scatter ($\sigma \approx 0.3$ dex) predicted by our model is still in excess of the typical $\sigma \approx 0.2$ dex value estimated from applying empirical models to observational data. We defer any further exploration of this issue to future work.

APPENDIX C: CRITERIA FOR A NON-EVOLVING SHM RELATION FOR STAR-FORMING GALAXIES

Here, we explore the conditions required for a non-evolving SHM relation for star-forming galaxies, based on the simplified analytical results presented in Section 4.1. There we assumed that the instantaneous star formation efficiency, $\eta_{\rm SF} \equiv \dot{M}_\star/(f_{\rm B}\dot{M}_{\rm H})$, scaled as $\beta_{\rm ml}^{-1}$, where $\beta_{\rm ml}$ is the mass loading factor for SNe feedback. By also assuming that the disc circular velocity scales with the halo circular velocity for haloes hosting star-forming galaxies, we arrived at the following relation:

$$\eta_{\rm SF} \propto M_{\rm H}^{\alpha_{\rm hot}/3}\,[\bar{\rho}_{\rm H}(a)]^{\alpha_{\rm hot}/6}\,. \tag{C1}$$

For a non-evolving SHM relation, $\eta_{\rm SF}$ should be constant at a fixed halo mass. Equation (C1) contradicts this requirement because the mean halo density, $\bar{\rho}_{\rm H}(a)$, depends on expansion factor, independent of halo mass. Integrating equation (C1) will therefore yield an evolving SHM relation.

In Section 4.1, we circumvented this problem by assuming that $\bar{\rho}_{\rm H}(a)$ was constant with expansion factor. In this case, integrating equation (C1) yields

$$M_\star \propto M_{\rm H}^{1+\alpha_{\rm hot}/3}\,[\bar{\rho}_{\rm H}]^{\alpha_{\rm hot}/6}\,, \tag{C2}$$

where, if $\bar{\rho}_{\rm H}$ is regarded as constant, we arrive at the non-evolving SHM relation given by equation (14). To test the regimes where this assumption is valid, we can invert the process of integrating equation (C1) into equation (C2), differentiating equation (C2) to give

$$\dot{M}_\star \propto \left(1+\frac{\alpha_{\rm hot}}{3}\right) M_{\rm H}^{\alpha_{\rm hot}/3}\dot{M}_{\rm H}\,[\bar{\rho}_{\rm H}]^{\alpha_{\rm hot}/6} + \frac{\alpha_{\rm hot}}{6} M_{\rm H}^{1+\alpha_{\rm hot}/3}\dot{\bar{\rho}}_{\rm H}\,[\bar{\rho}_{\rm H}]^{\alpha_{\rm hot}/6-1}\,.$$

In order for this to be equivalent to equation (C1), we require that

$$\frac{|\dot{M}_{\rm H}|}{M_{\rm H}} \gg F(a) \equiv \frac{\alpha_{\rm hot}}{2(3+\alpha_{\rm hot})}\frac{|\dot{\bar{\rho}}_{\rm H}(a)|}{\bar{\rho}_{\rm H}(a)}. \tag{C3}$$

In other words, given equation (C1), a non-evolving SHM relation requires that haloes are growing faster in mass than the rate with which they are changing in density. This inequality will not be satisfied in general. However, it may be satisfied for haloes of a particular mass over some redshift range.

In Fig. C1, we show, for a range of halo masses, the redshift range for which the inequality given by equation (C3) is satisfied. Here, we have selected haloes from our reference model that host star-forming galaxies at a given redshift, and then computed $\dot{M}_{\rm H}$, averaged over bins in halo mass. To calculate $|\dot{\bar{\rho}}_{\rm H}(a)|$, we consider both $\bar{\rho}_{\rm H}(a)$ calculated using the spherical collapse model (solid lines) and calculated directly using halo circular velocities taken from our reference model (dashed lines).

Starting with halo densities computed from the spherical collapse model, Fig. C1 shows that that the SHM relation should be non-evolving for star-forming galaxies when $z > 1$. The exact redshift where equation (C3) is met depends on halo mass, such that the inequality is met over a wider redshift range for more massive haloes.

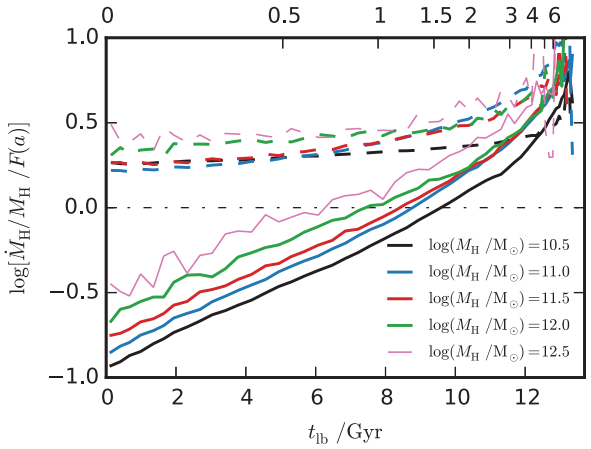

Figure C1. Scaled ratio of average halo accretion rates to the rate with which the mean halo density, $\bar{\rho}_{\rm H}$, is changing with time, plotted as a function of lookback time. Average halo formation rates are taken from our reference model for haloes that host star-forming central galaxies at a given redshift. The scaled rate of change in mean halo density, $F(a)$, is defined by equation (C3). Solid lines show $\dot{M}_{\rm H}/M_{\rm H}/F(a)$ when $F(a)$ is calculated using mean halo densities evaluated from the spherical collapse model. Dashed lines show $\dot{M}_{\rm H}/M_{\rm H}/F(a)$ when $F(a)$ is calculated by averaging over the mean halo densities taken directly from GALFORM. Each coloured line corresponds to a different halo mass bin, as labelled. The black dash–dotted horizontal line shows the line of equality, above which the condition for a non-evolving SHM relation is met for star-forming galaxies.

Conversely, from Fig. C1, we also expect that the SHM relation should evolve at lower redshifts ($z < 1$) if halo densities are computed using the spherical collapse model. However, significant evolution is not seen in the SHM relation over this redshift range (in the halo mass range associated with star-forming galaxies) for our reference model in, for example, Fig. 8. This can partially be explained by noting that for $z < 1$, star formation rates and halo mass accretion rates at a given halo mass have dropped dramatically relative to higher redshifts.

However, another very important consideration is that in our reference model, halo circular velocities (and hence the mean densities of haloes at fixed halo mass) of individual haloes are only updated when haloes double in mass. While halo formation (mass doubling) events are very frequent at high redshift when halo mass accretion rates are very large, they become very infrequent at low redshifts, for which halo mass accretion rates have dropped dramatically. Consequently, the average halo density for haloes from our reference model will evolve more slowly with time than if the halo densities followed exactly the spherical collapse model. This effect can be seen directly by considering the dashed lines in Fig. C1, which show $F(M_{\rm H}, a)$ evaluated from the average of halo densities taken directly from our reference model. In this case, it is apparent that the inequality given by equation (C3), on average, is met for all haloes over all redshifts. This helps to explain why the SHM model does not evolve significantly in our reference model.

APPENDIX D: AGN FEEDBACK AND THE SHM BREAK MASS

In Section 4.2, we derived a simple expectation for how a threshold halo mass for AGN feedback to be effective in suppressing cooling in hydrostatic haloes would evolve with cosmic time. To do so, we evaluated a criterion for quasi-hydrostatic equilibrium by equating the cooling time at the mean gas density within a halo to the freefall

time at the halo virial radius. Here, we present a more detailed derivation of this threshold halo mass, this time assuming a simple isothermal sphere density profile to evaluate equation (15) at the cooling radius. We also explore the role of the secondary criterion for effective AGN feedback in our model, which is that the AGN power must be sufficient to offset radiative cooling from a quasi-hydrostatic halo.

D1 Isothermal sphere derivation

As described in Section 4.2, for AGN feedback to be effective at shutting down cooling we require the cooling time, $t_{\rm cool}$, to exceed the freefall time, $t_{\rm ff}$, by a factor $\alpha_{\rm cool}^{-1}$,

$$t_{\rm cool}(r = r_{\rm cool}) \geq t_{\rm ff}(r = r_{\rm cool})/\alpha_{\rm cool}. \tag{D1}$$

We want to find a threshold halo mass, $M_{\rm H}(z)$, where this condition is met. To do this, we first need to compute $r_{\rm cool}$ in terms of $t_{\rm cool}$. The cooling time-scales as

$$t_{\rm cool}(r = r_{\rm cool}) \propto \frac{T}{\rho(r = r_{\rm cool})\Lambda_{\rm cool}(T, Z_{\rm g})}, \tag{D2}$$

and the virial temperature scales as

$$T \propto V_{\rm H}^2 \propto \frac{M_{\rm H}}{r_{\rm H}}. \tag{D3}$$

If we assume that the mass distribution within a halo follows an isothermal sphere profile (truncated at the virial radius, $r_{\rm H}$) such that

$$\rho(r) \propto \frac{M_{\rm H}}{r_{\rm H}\, r^2}, \tag{D4}$$

then we can evaluate equation (D2), yielding

$$t_{\rm cool}(r = r_{\rm cool}) \propto \frac{r_{\rm cool}^2}{\Lambda_{\rm cool}(T, Z_{\rm g})}. \tag{D5}$$

Rearranging, we find that the cooling radius scales as

$$r_{\rm cool} \propto \sqrt{t_{\rm cool}\Lambda_{\rm cool}(T, Z_{\rm g})}. \tag{D6}$$

To evaluate this expression, we need a value for $t_{\rm cool}$. In GALFORM, this is the time since the last halo formation event, $t_{\rm form}$. For the halo merger trees extracted from the MR7 simulation, we find this can be well described by

$$t_{\rm form} \propto t_{\rm H} M_{\rm H}^{0.05}, \tag{D7}$$

where $t_{\rm H} = 1/H(t)$ is the Hubble time.

For an isothermal sphere, the freefall time from a radius, r, (which must be within the virial radius) scales as

$$t_{\rm ff}(r) \propto \frac{r}{V_{\rm H}} \propto \frac{r}{M_{\rm H}^{1/3}\bar{\rho}_{\rm H}^{1/6}}. \tag{D8}$$

We now have everything required to evaluate equation (D1),

$$t_{\rm H} M_{\rm H}^{0.05} \propto \frac{r_{\rm cool}}{M_{\rm H}^{1/3}\bar{\rho}_{\rm H}^{1/6}}. \tag{D9}$$

Substituting for $r_{\rm cool}$ yields

$$t_{\rm H} M_{\rm H}^{0.05} \propto \frac{\sqrt{t_{\rm H} M_{\rm H}^{0.05}\Lambda_{\rm cool}(T, Z_{\rm g})}}{M_{\rm H}^{1/3}\bar{\rho}_{\rm H}^{1/6}}. \tag{D10}$$

We also need to evaluate the mean halo density using the spherical collapse model

$$\bar{\rho}_{\rm H}(z) \propto \Delta_{\rm c}(z)\rho_{\rm crit}(z) \propto \Delta_{\rm c}(z) t_{\rm H}^{-2}. \tag{D11}$$

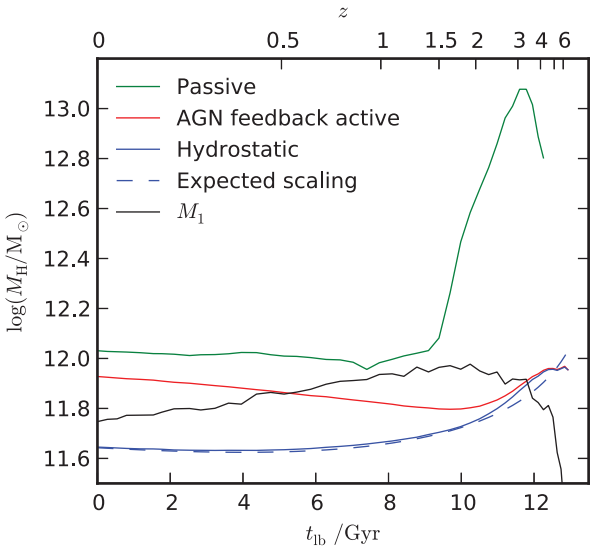

Figure D1. Halo mass thresholds plotted as a function of lookback time for our reference model. The green line shows the halo mass at which half of central galaxies are passive. The red line shows the halo mass for which AGN feedback is actively suppressing cooling in half of the haloes hosting central galaxies. The blue solid line shows the halo mass for which half of the haloes hosting central galaxies meet the quasi-hydrostatic equilibrium criterion for AGN feedback given by equation (D1). The dashed blue line shows the redshift scaling given by equation (D12), normalized to agree with the solid blue line at $z = 0$. The solid black line shows the break halo mass in the median SHM relation, M_1, for our reference model.

Equation (D10) then reduces to

$$M_{\rm H} \propto \Lambda_{\rm cool}(T, Z_{\rm g})^{1.4}\, \Delta_{\rm c}(z)^{-0.47}\, t_{\rm H}^{-0.47}. \tag{D12}$$

This scaling is close to the simplified derivation presented in Section 4.2, which, for reference, yielded $M_{\rm H} \propto \Lambda_{\rm cool}(T, Z_{\rm g})^{1.5}\, \Delta_{\rm c}(z)^{1/4}\, t_{\rm H}^{-0.5}$. The two derivations differ approximately by a factor of $\Delta_{\rm c}(z)^{3/4}$, which turns out to be unimportant relative to the evolution in the cooling function, $\Lambda_{\rm cool}(T, Z_{\rm g})$.

D2 Hydrostatic equilibrium, AGN feedback and quenching

To check whether equation (D12) is a reasonable description of what occurs in GALFORM, we compute the halo mass where the fraction of central galaxies that meet the quasi-hydrostatic equilibrium criterion given by equation (D1) is equal to 0.5. The resulting halo mass (solid blue line) is compared to the expectation from equation (D12) (dashed blue line) in Fig. D1. To evaluate equation (D12), we take the median gas temperature and metallicity at the halo mass given by the solid blue line to compute the evolution of the cooling function. From Fig. D1, it is apparent that the halo mass where the hydrostatic criterion is met is essentially constant up to $z = 2$ and then increases mildly for $z > 2$.

For the AGN feedback model in GALFORM, a second requirement for AGN feedback to be effective in suppressing cooling is that the maximum AGN power (taken to be a fraction of the Eddington luminosity of the black hole) is sufficient to balance the radiative luminosity of the cooling flow (Bower et al. 2006). In practice, provided that the central galaxy hosts a central supermassive black hole, this criterion is almost always met, such that the hydrostatic criterion given by equation (D1) controls whether AGN feedback is effective in a given halo. However, there is a non-negligible fraction of central galaxies in our model in haloes close the hydrostatic

threshold mass given by equation (D12) that do not host supermassive black holes. These are the model galaxies that have not undergone a gas-rich merger or a disc instability over their lifetime, and typically have bulge-to-total ratios ≈0. As a consequence of this galaxy population, the threshold halo mass where AGN feedback is active in suppressing cooling in half of the haloes hosting central galaxies (solid red line in Fig. D1) is actually larger than the mass where the hydrostatic equilibrium criterion is met (solid blue line).

Another consideration is that once AGN feedback becomes active in a given halo at suppressing gas inflow on to the central galaxy, there can still be an appreciable delay before star formation shuts down in that galaxy. The length of the delay depends primarily on the strength of SNe feedback in ejecting cold gas from the central galaxy. The solid green line in Fig. D1 shows the halo mass above which half of the central galaxies are passive. Below $z = 2$, this mass closely traces (with an offset) the halo mass where AGN feedback is active. However, for $z > 2$, the halo mass above which central galaxies are typically quenched increases strongly with redshift. This strong evolution for $z > 2$ is not reflected by a corresponding evolution in the SHM break mass, M_1, which we overplot in Fig. D1 (solid black line). We attribute this difference primarily to the fact that the width of the sigmoid function that describes the passive fraction of central galaxies as a function of halo mass is significantly larger at high redshift compared to low redshift. As such, at high redshift, there is a non-negligible population of passive central galaxies at significantly lower halo masses than is indicated by the red line in Fig. D1 (which shows the halo mass where the sigmoid function is equal to 0.5).

This paper has been typeset from a TEX/LATEX file prepared by the author.